ACCSCIENCE PUBLISHING

International Journal of Bioprinting

REVIEW ARTICLE

Bioprinting and artificial intelligence strategies for additively manufactured wearable biosensors

Zhuoyuan Yang[1†], Zefu Ren[1†], Yuxuan Wu[1†], Meng Cheng[2,3,4*], Jia An[5], Sirish Namilae[1*], Chee Kai Chua[2,3,4*], and Yizhou Jiang[1*]

[1]Department of Aerospace Engineering, Embry-Riddle Aeronautical University, Daytona Beach, Florida 32114, United States of America

[2]Key Laboratory of Metallurgical Equipment and Control Technology, Ministry of Education, Wuhan University of Science and Technology, Wuhan, Hubei 430081, China

[3]Precision Manufacturing Institute, Wuhan University of Science and Technology, Wuhan, Hubei 430081, China

[4]Hubei Key Laboratory of Mechanical Transmission and Manufacturing Engineering, Wuhan University of Science and Technology, Wuhan 430081, China

[5]Engineering Product Development Pillar, Singapore University of Technology and Design, 8 Somapah Road, Singapore 487372, Singapore

[†]*These authors contributed equally to this work.*

***Corresponding authors:**
Meng Cheng (chengmeng@wust.edu.cn);
Sirish Namilae (sirish.namilae@erau.edu);
Chee Kai Chua (cheekai@wust.edu.cn);
Yizhou Jiang (yizhou.jiang@erau.edu)

Citation: Yang Z, Ren Z, Wu Y, *et al*. Bioprinting and artificial intelligence strategies for additively manufactured wearable biosensors. *Int J Bioprint*. 2026;12(5):026260276. doi: 10.36922/IJB026260276

Received: June 28, 2026

1st revised: July 26, 2026

2nd revised: August 21, 2026

3rd revised: August 30, 2026

Accepted: September 3, 2026

Published online: September 7, 2026

Copyright: © 2026 Author(s). This is an Open-Access article distributed under the terms of the Creative Commons Attribution License, permitting distribution, and reproduction in any medium, provided the original work is properly cited.

Publisher's Note: AccScience Publishing remains neutral with regard to jurisdictional claims in published maps and institutional affiliations.

Abstract

Additively manufactured wearable biosensors enable continuous, noninvasive, and real-time monitoring of physiological and biochemical signals during daily use. Recent advances in artificial intelligence (AI) provide complementary tools for identifying printable material windows, optimizing formulations and printing parameters, monitoring fabrication quality, and interpreting noisy, high-dimensional sensing data. These capabilities are particularly relevant to wearable biosensors, whose performance depends on manufacturing reproducibility and reliable signal analysis during continuous or multimodal operation. This review summarizes recent progress in the AI-assisted development of additively manufactured wearable biosensors across three stages: pre-printing design, in-process monitoring and control, and post-printing signal interpretation and application. By organizing the field around this workflow, we clarify how AI supports material selection, fabrication optimization, device evaluation, and wearable sensing, and identify the remaining challenges in developing more reliable and adaptive biosensing systems.

Keywords: Artificial intelligence; Additive manufacturing; Wearable biosensors; Biomaterials; Bioprinting; Biosignals

1. Introduction

Wearable biosensors provide a promising route for continuous, noninvasive, and *in situ* monitoring of human health.[1-6] By integrating sensing components with soft and body-compatible interfaces, these devices can capture physiological and biochemical information directly from the body, including strain, pressure, pulse, respiration, temperature, sweat metabolites, electrolytes, wound biomarkers, and interstitial fluid biomarkers.[7-11] Additive manufacturing (AM) has expanded the design space of

wearable biosensors by enabling customized geometries, spatial material patterning, and integrated three-dimensional structures that are difficult to achieve using conventional planar fabrication.[2,12-20] Deposition-based printing methods, such as direct ink writing (DIW), inkjet printing, fused deposition modeling (FDM), screen printing, electrohydrodynamic printing (EHD printing), and aerosol jet printing (AJP), can process conductive inks, hydrogels, elastomers, thermoplastic polymers, and biofunctional materials.[14-16,21-32] Photopolymerization-based methods, including stereolithography (SLA), digital light processing (DLP), two-photon polymerization (2PP), and volumetric 3D printing, are well-suited for fabricating microneedles, microfluidic structures, porous interfaces, and high-resolution device components.[33-45] These printing strategies allow wearable biosensors to be designed with controlled geometry, material distribution, and skin-compatible interfaces.

Although AM has improved the design and fabrication of wearable biosensors, AM-fabricated devices still need to meet interconnected requirements in material selection, printing reproducibility, device performance, and signal interpretation.[46-48] Their performance depends on coupled relationships among material composition, ink rheology, printing parameters, printed architecture, biofunctional activity, and wearable sensing environments.[2,49,50] While some of these relationships primarily govern processing behavior, others continue to play a critical role during real-time use, where motion artifacts, sweat dynamics, environmental variations, device deformation, and user-to-user variability can distort sensor responses and affect their accuracy.[17,51] Reliable deployment therefore requires data-driven methods that connect material design, AM process optimization, device performance prediction, and wearable signal interpretation.

Recent advances in artificial intelligence (AI) provide these data-driven methods by learning from complex experimental and sensing datasets and using them for prediction, classification, optimization, perception, and decision support.[52-55] This capability is useful because material characteristics, AM parameters, printed structures, device performance, and sensing signals are often coupled through nonlinear and multivariable relationships.[56-59] AI-assisted bioprinting addresses a closely related manufacturing problem: the formulation and processing of soft functional materials affect both printability and the function of the printed structure.[31,47] Data-driven studies in bioprinting have used AI to relate material formulation and rheological behavior to printability and processing conditions.[60,61] This modeling approach can therefore be transferred to wearable biosensor manufacturing, where material and process decisions also influence sensor integration and functional performance.

At the pre-printing design stage, AI models can help define the initial material, process, and structural design space before fabrication. The input descriptors may include composition, rheological behavior, processability, photoreactivity, curing behavior, functional properties, mechanical properties, interfacial behavior, biological activity, printing parameters, target geometry, and image- or simulation-derived features.[62] Recent studies relevant to AM-fabricated wearable biosensors have used AI to predict biomaterial printability from formulation and processing data, identify material and process windows, optimize droplet or filament formation, and guide the development of inks, resins, hydrogels, bioinks, and functional composites across AM platforms.[52,60,63-65] These models can reduce trial and error during early design and identify descriptors associated with processability, printability, curing quality, and structural fidelity.[53] This is especially relevant for AM wearable biosensors, where pre-printing design must balance printable materials with device-level requirements, including flexibility, electrical performance, biocompatibility, interfacial adhesion, geometric fidelity, analyte transport, and sensing activity.[56,61]

At the process control stage, AI can link AM parameters, printed structures, and fabrication quality metrics for prediction and control. Machine learning (ML), computer vision (CV), and deep learning (DL) have been used for image-based defect detection and real-time error recognition in extrusion-based AM. These methods can detect unstable extrusion, poor line quality, structural distortion, and departures from stable printing conditions.[14,62,66-70] Regression and optimization models also relate processing variables to printed feature quality, including line width, porosity, surface morphology, interlayer adhesion, and structural fidelity.[25,71,72] AI can also link printed device architecture, process-induced structural features, and biosensor outputs to sensing performance.[17,44,73,74] AM-fabricated wearable biosensors often contain printed electrodes, serpentine interconnects, microneedle arrays, microfluidic channels, porous layers, and multilayer soft interfaces.[75] Small changes in these structures can alter charge transfer, fluid sampling, mechanical compliance, skin contact, and analyte transport.[76,77] AI models can map structural descriptors to device-level outputs, including conductivity, sensitivity, limit of detection, response time, hysteresis, and durability.[78]

At the post-printing application stage, AI is also used for signal interpretation.[57,58] AM-fabricated wearable biosensors can generate electrochemical, mechanical,

optical, thermal, and environmental signals under dynamic body conditions.[27,40,56] These signals are often noisy and nonlinear, and they can be affected by user motion, device deformation, skin contact, sweat dynamics, and environmental changes.[12,79,80] AI has been applied to several biosensing modalities. In fluorometric and colorimetric biosensing, image-based AI can improve point-of-care analysis when image acquisition conditions are not ideal.[42] In electrochemical biosensing, AI can extract analyte information from low signal-to-noise data, compensate for nonlinear responses, and separate target signals from interfering compounds.[80] In continuous wearable sensing, AI has been used to combine impedance data with skin temperature and humidity for sweat glucose prediction.[17,74] For AM-fabricated wearable biosensors, these functions support denoising, drift correction, feature extraction, biomarker prediction, multimodal fusion, and personalized calibration.[27,40,42,56]

These needs have increased interest in integrating AI with AM-fabricated wearable biosensors, as illustrated by the workflow in Figure 1 and the recent Scopus publication trends in Figure 2. Existing reviews usually discuss wearable biosensors, AM fabrication, and AI-assisted biosensing as separate topics. A workflow-level framework is needed to explain how AI supports the development of AM-fabricated wearable biosensors from material design to device use. Here, the presented review focuses on AI for AM-fabricated wearable biosensors, with AI treated as the main data-driven approach throughout the article. We first introduce the foundations of wearable biosensors, AM strategies, and AI workflows. We then review recent progress in AI-assisted material design and printability optimization, process monitoring and fabrication quality control, device architecture and performance optimization, and signal interpretation for wearable applications. We close by discussing challenges and outlooks for integrated AI-enabled AM wearable biosensors, including structured data frameworks, multifunctional material optimization, broader AM-process coverage, closed-loop process control, digital twins, interpretable and reliable models, long-term validation, and deployable edge intelligence.

2. Foundations of AI in additively manufactured wearable biosensors

2.1. AI overview

This section provides a brief overview of AI, with more detailed discussions available in previous reviews.[56-58] AI generally describes computational methods that perform tasks such as perception, pattern recognition, prediction, optimization, reasoning, and decision-making. In AM-fabricated wearable biosensors, most current AI applications rely on ML, DL, Bayesian optimization, CV, and multimodal data analysis.[8,9,26,34,38,46,58,60,61,80-83] We therefore focus on ML principles while keeping them within the broader AI framework.

AI algorithms can learn from data through supervised, unsupervised, or semi-supervised approaches.[56,59,80,84] Supervised learning uses labeled data with known outputs and is commonly used for regression and classification. Regression predicts continuous variables, such as concentration, conductivity, sensitivity, or response time. Classification assigns samples to discrete categories, such as positive or negative, printable or non-printable, defective or non-defective, and normal or abnormal.[16] Unsupervised learning uses unlabeled data to identify hidden patterns, clusters, or low-dimensional representations, and is often used for clustering, feature extraction, anomaly detection, and dimensionality reduction.[78,85] Semi-supervised learning combines labeled and unlabeled data, which is useful when labeled experimental data are limited.[56] ML models can also work with unimodal or multimodal data. Unimodal ML analyzes one data source, whereas multimodal ML integrates multiple data sources to improve prediction or decision reliability.

2.1.1. Data-driven AI

In data-driven AI, models are usually developed through a workflow that includes data collection, preprocessing, feature extraction or selection, model selection, training, validation, testing, and performance evaluation.[59,86,87] Raw data can come from experiments, images, sensors, simulations, or databases. These data are usually preprocessed to remove noise, correct artifacts, handle missing values, normalize feature scales, and reduce the effect of outliers. Feature extraction or dimensionality reduction can then be used to retain useful information while lowering data complexity. The dataset is commonly divided into training, validation, and testing sets.[59] The training set is used to fit model parameters, the validation set is used for hyperparameter tuning and model selection, and the testing set is used to evaluate performance on unseen data. For small datasets, cross-validation can provide a more stable estimate of model generalization. Model performance should be assessed with task-specific metrics. Common metrics include accuracy, precision, recall, F1 score, and area under the receiver operating characteristic (ROC) curve for classification, and coefficient of determination, mean absolute error (MAE), mean squared error (MSE), and root mean squared error (RMSE) for regression. Careful validation is needed because overfitting, data leakage, biased sampling, and limited external testing can produce overly optimistic performance estimates.[59] This concern is especially relevant

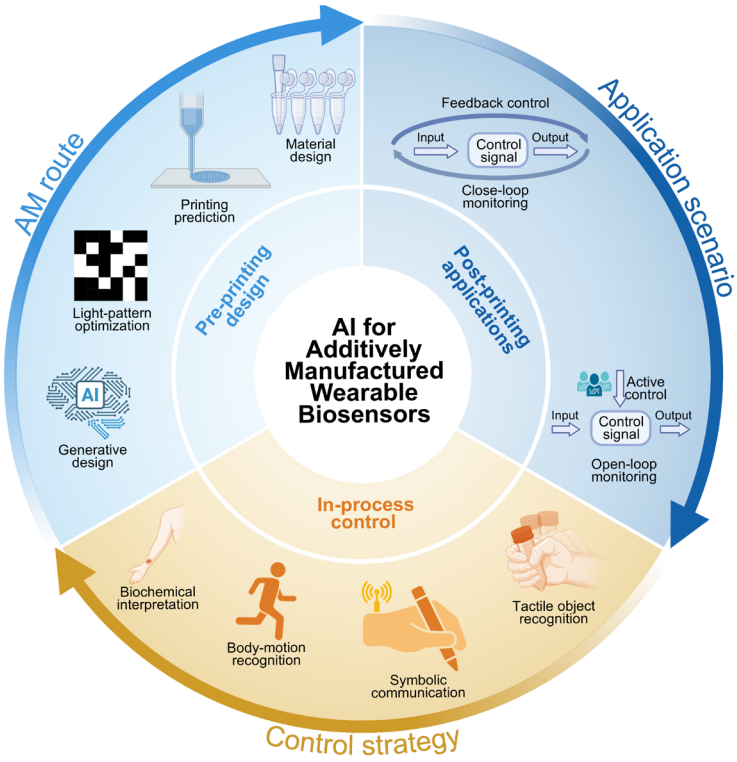


Figure 1. Stage-specific AI framework for additively manufactured wearable biosensors
Abbreviations: AI: Artificial intelligence; AM: Additive manufacturing.

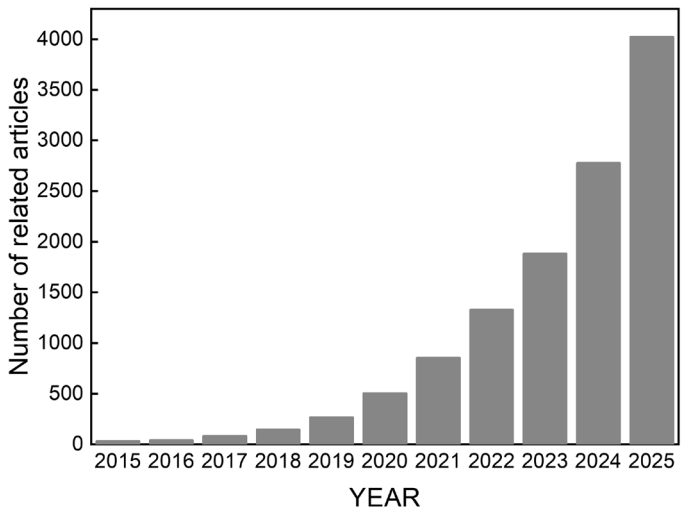


Figure 2. Publication trends of AI for additively manufactured wearable biosensors from 2015 to 2025 (in the Scopus database)
Abbreviation: AI: Artificial intelligence.

to AM-fabricated wearable biosensors, where datasets are often small, heterogeneous, and affected by device-to-device and user-to-user variability.[56]

Although the main AI workflow is similar across models, learning algorithms differ in structure, complexity, data requirements, and interpretability (Table 1).[46,56,59]

Table 1. Representative data-driven AI algorithms for additively manufactured wearable biosensors

AI Algorithm	Main task	Strengths	Limitations
SVM	Classification, regression	Good for small datasets	Less efficient for large noisy data
RF	Classification, regression	Robust, interpretable feature importance	Lower transparency with many trees
XGBoost	Classification, regression	Strong tabular prediction	Needs tuning
ANN	Nonlinear prediction	Flexible modeling	Requires tuning
CNN	Image analysis	Spatial feature extraction	Needs image datasets
RNN/LSTM	Time series	Temporal modeling	Training complexity
Autoencoder	Denoising, feature extraction	Compact representation	Interpretation limited
Transformer	Sequence, multimodal data	Long-range dependencies	Data intensive
PCA	Dimensionality reduction	Visualization, feature compression	Linear method

Abbreviations: AI: Artificial intelligence; ANN: Artificial neural network; CNN: Convolutional neural network; LSTM: Long short-term memory; PCA: Principal component analysis; RF: Random forest; RNN: Recurrent neural network; SVM: Support vector machine; XGBoost: Extreme gradient boosting.

Common models used in this field include shallow ML models and DL models. Shallow models, such as support vector machines (SVMs), decision trees (DTs), random forests (RFs), gradient-boosted trees, K-nearest neighbors (KNN), and shallow artificial neural networks, usually rely on predefined features and have fewer trainable parameters.[59,88] These models are often suitable for small or structured datasets and are usually easier to train and interpret. DL models use multiple hidden layers to learn hierarchical representations from raw or high-dimensional data. They are effective for image, signal, and sequence analysis, but they usually require larger datasets, higher computational cost, and careful validation to reduce overfitting. The algorithm should therefore be selected based on the learning task, data structure, dataset size, and need for interpretability.

Support vector machines (SVMs) are supervised learning models used for classification and regression.[89] In classification, an SVM searches for a decision boundary that separates classes with the largest margin. Kernel functions allow SVMs to handle nonlinear data by mapping the input into a higher-dimensional feature space. Support vector regression applies a related principle to continuous output prediction. SVMs are useful for relatively small datasets with clear class boundaries, but their performance may decrease when the data are noisy, strongly overlapping, or very large.

Decision trees (DTs) make predictions through a sequence of feature-based splitting rules.[90] Each split divides the data according to a selected feature, and the final prediction is made at a terminal leaf node. DTs are intuitive and interpretable, but a single tree can be sensitive to noise and prone to overfitting. RFs reduce this problem by building many DTs and combining their outputs. Classification is usually based on majority voting, whereas regression is based on averaged predictions from multiple trees. RFs can capture nonlinear relationships and handle mixed input variables, although large forests may increase computational cost and reduce transparency.[88]

Gradient boosting is another tree-based ensemble method.[91] Unlike RFs, which build trees independently, gradient boosting builds trees sequentially. Each new tree corrects residual errors from the previous model. Gradient-boosted trees and eXtreme Gradient Boosting (XGBoost) are widely used for structured datasets because they often provide strong predictive performance. XGBoost also improves training efficiency and uses regularization to limit overfitting. These methods can be used for both classification and regression, but their performance depends on hyperparameters such as learning rate, tree depth, number of estimators, and regularization strength.

K-nearest neighbors (KNN) is an instance-based learning method.[92] For a new sample, KNN identifies the k most similar samples in the training dataset using a defined distance metric. Classification is determined by voting among neighboring samples, whereas regression is calculated from nearby sample values. KNN is easy to implement and does not require an explicit training stage. However, it is sensitive to feature scaling, the choice of k, and the distance metric. It can also become inefficient for

large datasets and less reliable in high-dimensional feature spaces.

Artificial neural networks (ANNs) are computational models composed of interconnected layers of nodes.[93] A typical ANN includes an input layer, one or more hidden layers, and an output layer. During training, the model adjusts the weights between nodes to minimize prediction error. Nonlinear activation functions allow ANNs to model complex input-output relationships. Shallow ANNs contain a small number of hidden layers, whereas deep neural networks contain many hidden layers and can learn more complex representations. Neural network performance depends strongly on architecture design, training data size, learning rate, regularization, and hyperparameter selection.

Convolutional neural networks (CNNs) are DL models designed for data with spatial structure, especially images.[94] They use convolutional filters to extract local features and preserve spatial relationships in the input data. CNNs are commonly used for image classification, object detection, segmentation, and microscopy image analysis. Recurrent neural networks (RNNs) are designed for sequential data because they retain information from previous time steps. Long short-term memory networks (LSTMs) and gated recurrent units (GRUs) improve the ability of RNNs to capture long-range temporal dependencies, making them useful for time-series analysis.

Autoencoders learn compact representations of input data. They usually include an encoder that compresses the input into a lower-dimensional latent space and a decoder that reconstructs the input from this latent representation. Autoencoders can be used for dimensionality reduction, denoising, anomaly detection, and feature extraction. Transformer-based models are also increasingly used for sequence and multimodal data analysis.[95] Their attention mechanisms can capture long-range relationships among different elements in a dataset, although they usually require large datasets and high computational cost.

Principal component analysis (PCA) is not a predictive ML model in the strict sense, but it is widely used in ML workflows for dimensionality reduction and feature extraction.[96] PCA transforms correlated input variables into a smaller number of orthogonal principal components that retain the dominant variance in the dataset. This can reduce data complexity, remove redundant features, support visualization, and lower the risk of overfitting. Other feature selection and dimensionality reduction methods can also be used to identify informative variables or improve model efficiency.

Optimization-oriented methods such as Bayesian optimization and active learning are useful when experiments are expensive or time-consuming.[97] Bayesian optimization uses a surrogate model to estimate the relationship between input variables and target performance, then selects the next experimental condition using an acquisition function. Active learning selects the most informative samples for labeling or experimentation. Both methods can reduce the number of trials needed for model-guided optimization.

Overall, different AI algorithms provide different balances among accuracy, interpretability, data demand, and computational cost. SVMs and KNN are often suitable for small datasets. Tree-based ensemble models are effective for structured data. Neural networks can model complex nonlinear relationships. CNNs are useful for image-based analysis, whereas RNNs, LSTMs, and GRUs are suitable for sequential sensing data. Autoencoders and transformers can support high-dimensional, noisy, or multimodal datasets. Together with Bayesian optimization and active learning, these methods provide the algorithmic basis for AI-assisted material design, process monitoring, device optimization, and signal interpretation in AM-fabricated wearable biosensors.

2.1.2. Generative AI

Generative AI refers to AI models that learn data distributions and create new outputs, including images, structures, sequences, graphs, and text.[98] This differs from predictive AI, which mainly maps input data to labels, properties, or process outcomes. In design tasks, this capability is often connected with generative design, where candidate solutions are generated under defined objectives and constraints. For additively manufactured wearable biosensors, generative AI is mainly relevant before fabrication. It can support the early exploration of material formulations, printable geometries, device layouts, and processing windows. Since wearable biosensors need to balance printability, mechanical compliance, biological compatibility, electrical or biochemical function, and sensing reliability, generated outputs should be treated as design candidates that require further validation.

Common generative model families include generative adversarial networks (GANs), variational autoencoders (VAEs), conditional variational autoencoders (CVAEs), diffusion models, large language models (LLMs), and vision-language models (VLMs) (Table 2). GANs use a generator-discriminator framework to create new samples from learned data distributions. VAEs encode data into latent spaces and generate new outputs by sampling from these spaces, while CVAEs add conditional inputs to guide the generation process. Diffusion models generate data by

Table 2. Representative generative AI models for additively manufactured wearable biosensors

Generative model	Main task	Strengths	Limitations
GANs	Image and structure generation	Realistic outputs	Unstable training
VAEs/CVAEs	Latent-space generation	Stable and controllable	Less sharp outputs
Diffusion models	Text- or image-guided generation	High-quality outputs	High computational cost
LLMs	Text generation	Knowledge extraction	Inaccurate content
VLMs	Image-text reasoning	Figure interpretation	Data-dependent performance

Abbreviations: AI: Artificial intelligence; CVAEs: Conditional variational autoencoders; GANs: Generative adversarial networks; LLMs: Large language models; VAEs: Variational autoencoders; VLMs: Vision-language models.

learning a denoising process and can be conditioned by text, images, or target properties. LLMs generate text-based outputs and can support literature mining, hypothesis generation, and design reasoning. VLMs connect visual and textual information, which is useful when design information is distributed across images, figures, captions, and written descriptions.

2.2. AM strategies for wearable biosensors

Additive manufacturing enables wearable biosensors by depositing, jetting, or curing functional materials at predefined locations to form device structures that are difficult to achieve with conventional methods.[29,30,99,100] For wearable biosensors, the printing strategy should be selected based on the target material, device geometry, sensing mechanism, and body-interface requirement. In this review, printing technologies are grouped according to their material-forming mechanism into deposition-based printing and photopolymerization-based printing (Table 3).[18] Deposition-based printing forms structures by placing inks, pastes, melts, gels, or biofunctional materials onto substrates or supporting matrices.[55,101] Photopolymerization-based printing forms structures by spatially controlling light-induced curing in photosensitive materials.[102] As summarized in Table 3, these strategies differ in printable materials, process variables, achievable structures, and sensing-related performance.[18]

2.2.1. Deposition-based printing

Deposition-based printing fabricates wearable biosensors by depositing functional inks, pastes, gels, melts, or bioactive materials onto flexible substrates or supporting matrices. This category includes DIW, inkjet printing, FDM, screen printing, EHD printing, and AJP. These methods are useful for wearable biosensors because they can process conductive materials, soft matrices, thermoplastic supports, and biofunctional inks under relatively mild or device-compatible conditions. They are commonly used to fabricate electrodes, conductive traces, sensing layers, flexible patches, device supports, and patterned functional interfaces.

Direct ink writing (DIW) is widely used to print conductive inks, conductive hydrogels, elastomers, ionogels, and biofunctional inks.[28,31] In this method, the material is extruded through a nozzle and deposited along a programmed path. Printing quality depends on material variables such as viscosity, filler content, conductivity, modulus, and bioactivity. It is also affected by process parameters, including nozzle diameter, printing pressure, printing speed, flow rate, layer height, and curing condition. These factors determine filament formation, printed line stability, and structural fidelity. For wearable biosensors, DIW is suitable for electrodes, conductive traces, hydrogel sensing layers, soft patches, and stretchable interconnects.[75,103,104] Its main advantage is the ability to print soft and functional materials with spatial control.

Inkjet printing is another deposition-based method, but it relies on controlled droplet generation rather than continuous extrusion.[83] It is suitable for low-viscosity conductive inks, PEDOT, metal nanoparticle inks, enzyme inks, and functional coatings. Key material variables include viscosity, surface tension, particle size, concentration, and bioactivity. Important process variables include droplet volume, jetting frequency, drop spacing, substrate temperature, and drying condition. Inkjet printing is used for patterned electrodes, localized coatings, sensing layers, and conductive traces.[105] Because it deposits small volumes of functional materials with good spatial resolution, it is useful for localized functionalization of wearable biosensors.

Compared with conventional inkjet printing, EHD printing uses an electric field to draw ink from a nozzle and form fine jets or droplets.[29,106,107] This electric-field-assisted

Table 3. Additive manufacturing strategies and key design variables for wearable biosensors

Category	Technology	Material selection	Material design	Printable structures	Process control	Sensing parameters
Deposition-based printing	DIW	Conductive inks Elastomers Biofunctional inks	Rheology Modulus Bioactivity	Electrodes Traces Patches	Printing pressure Printing speed Layer height	Sensitivity Stretchability Signal stability
	Inkjet	Conductive inks Metal nanoparticle inks Enzyme inks	Viscosity Surface tension Concentration	Electrodes Coatings Sensing layers	Droplet volume Jetting frequency Drop spacing	Sensitivity Selectivity Signal repeatability
	EHD printing	Conductive inks Polymer solutions Biofunctional inks	Conductivity Viscosity Surface tension	Microelectrodes Microfibers Electrode arrays	Voltage Flow rate Standoff distance	Resolution Sensitivity Response time
	AJP	Nanoparticle inks Biofunctional inks	Ink stability Particle size Solvent volatility	Fine traces Microelectrodes Interconnects	Atomizer flow Sheath gas Standoff distance	Line resolution Conductivity Mechanical stability
	FDM	Thermoplastic polymers	Melt flow Filler content Biocompatibility	Substrates Housings Supports	Temperature Speed Nozzle size	Wearability Mechanical stability Device integration
	Screen printing	Conductive inks Enzyme inks Functional coatings	Viscosity Adhesion Curing behavior	Electrodes Sensing layers Patches	Mesh size Squeegee speed Drying condition	Sensitivity Selectivity Repeatability
Photopolymerization-based printing	SLA/DLP	Photocurable hydrogels Functional resins Biocompatible resins	Curing behavior Modulus Biocompatibility	Microneedles Microfluidics Porous structures	Light intensity Exposure time Resolution	Shape fidelity Analyte diffusion Signal repeatability
	2PP	Photocurable resins Hydrogel precursors Functional polymers	Transparency Photoactivity Biocompatibility	Microstructures Microneedles Nanostructures	Laser power Scan speed Voxel size	Spatial resolution Interface stability Analyte transport
	Volumetric printing	Photocurable resins Hydrogel precursors Functional polymers	Transparency Curing kinetics Biocompatibility	Soft constructs Channels Soft interfaces	Light dose Projection angle Exposure time	Shape fidelity Cell viability Mass transport

Abbreviations: 2PP: Two-photon polymerization; AJP: Aerosol jet printing; DIW: Direct ink writing; DLP: Digital light processing; EHD: Electrohydrodynamic; FDM: Fused deposition modeling; SLA: Stereolithography.

mechanism allows precise deposition of conductive polymer, nanocomposite, hydrogel, and biofunctional inks. Key variables include viscosity, electrical conductivity, surface tension, applied voltage, flow rate, nozzle-substrate distance, and stage speed. For wearable biosensors, EHD printing is suitable for electrodes, microelectrode arrays, microfibers, and patterned sensing layers that require fine spatial resolution.

Aerosol jet printing (AJP) is another direct-write method for printed electronics and wearable sensing devices. In AJP, the ink is atomized into an aerosol and focused by a sheath gas before deposition. This differs from conventional inkjet printing, which ejects droplets directly from a printhead. AJP can print conductive inks, nanoparticle inks, polymer inks, and biofunctional inks on planar or curved substrates. Important process variables include atomizer flow, carrier gas flow, sheath gas flow, standoff distance, printing speed, and post-treatment condition. For wearable biosensors, AJP is suitable for fine conductive traces, microelectrodes, interconnects, and conformal sensing patterns.

Fused deposition modeling (FDM) uses thermoplastic filaments rather than liquid inks and is commonly used to print structural components for wearable biosensors. These components include flexible substrates, device supports, sensor housings, microneedle structures, wristbands, and customized wearable interfaces.[14,25,108,109] Typical materials include thermoplastic polyurethane (TPU), polylactic acid (PLA), polycaprolactone (PCL), conductive thermoplastic filaments, carbon-filled polymers, and other functional polymer composites. Material variables include melting temperature, flexibility, conductivity, filler content, stiffness, and biocompatibility. Process parameters such as nozzle temperature, bed temperature, printing speed, infill density, layer height, and cooling condition affect dimensional accuracy, interlayer bonding, flexibility, and mechanical robustness. For wearable biosensors, FDM is useful when the device requires customized geometry, structural support, or mechanically stable integration with sensing components.

Screen printing is also a deposition-based method because it deposits functional inks through a patterned screen.[110,111] It is widely used for wearable electrochemical biosensors and can fabricate carbon electrodes, Ag/AgCl electrodes, conductive traces, enzyme layers, and functional coatings in a scalable manner. Common materials include carbon inks, Ag/AgCl inks, conductive pastes, enzyme inks, and functional coatings. Important material variables include viscosity, particle size, conductivity, adhesion, and bioactivity. Process control involves mesh size, squeegee speed, printing pressure, drying condition, and layer thickness. Screen printing is suitable for electrodes, electrode arrays, conductive traces, coatings, and flexible patches.

2.2.2. Photopolymerization-based printing

Photopolymerization-based printing forms three-dimensional structures by selectively curing photocurable materials with patterned or focused light.[44] Compared with deposition-based printing, this strategy is more suitable for high-resolution structures, complex three-dimensional geometries, and miniaturized components. It is particularly relevant to wearable biosensors that require microneedles, microfluidics, porous structures, and structured sensing interfaces.

Stereolithography (SLA) and digital light processing (DLP) are commonly used to fabricate biosensor-related structures.[34-39,43,112] These methods can process photocurable hydrogels, poly(ethylene glycol) diacrylate (PEGDA), gelatin methacryloyl (GelMA), functional resins, and biocompatible resins. Material variables include photoinitiator content, curing behavior, modulus, swelling, and biocompatibility. Process parameters include light intensity, exposure time, layer thickness, resolution, and post-curing. For wearable biosensors, photopolymerization-based methods are suitable for microneedles, microfluidic structures, chambers, porous structures, and structured interfaces. These structures can support interstitial fluid sampling, sweat transport, analyte diffusion, and controlled sensing environments.

Two-photon polymerization provides higher spatial resolution than conventional SLA or DLP by using a focused laser to polymerize materials within a small voxel.[113-115] It is suitable for photocurable resins, hydrogel precursors, and functional polymers. Key material variables include photoactivity, modulus, transparency, and biocompatibility. Process parameters include laser power, scan speed, voxel size, and writing path. Two-photon polymerization can fabricate microneedles, high-resolution sensing interfaces, and micro- or nanoscale structures. Although its throughput is limited, it is useful for miniaturized sensing components that require fine structural control.

Volumetric 3D printing is another photopolymerization-based method that forms 3D structures inside a photosensitive resin volume through controlled light exposure.[116,117] Unlike layer-by-layer SLA or DLP, it can cure a complete 3D geometry within the resin volume. Typical materials include photocurable resins, biocompatible photopolymers, and cell-laden hydrogels. Important factors include optical transparency, curing kinetics, light absorption, light dose, projection angle, exposure time, and rotation speed. For wearable biosensors, volumetric 3D printing is relevant to soft 3D hydrogel constructs, embedded channels, body-conformal interfaces, and porous sensing structures.

Overall, deposition-based printing and photopolymerization-based printing provide complementary routes for fabricating wearable biosensors. Deposition-based methods are suitable for conductive inks, soft materials, biofunctional coatings, and flexible electrode structures. Photopolymerization-based methods are better suited for microneedles, microfluidics, porous architectures, and high-resolution three-dimensional structures. The variables listed in Table 3 also show why AI is useful in this field. Material selection, formulation design, process control, sensing parameters, and printable structures are strongly coupled, making them difficult to optimize by trial and error alone. This relationship provides the basis for ML-guided material design, ML-assisted process control, and ML-driven device performance optimization discussed in the following sections.

3. AI for additively manufactured wearable biosensors

The development of AM-fabricated wearable biosensors can be organized into a three-stage AI-assisted workflow comprising pre-printing design, in-process monitoring and control, and post-printing analysis and applications (Figure 3). Before fabrication, AI supports material selection, formulation design, printability prediction, process-window selection, and light-pattern optimization. During printing, AI uses fabrication data to monitor process stability, detect defects, and guide parameter adjustment through open-loop optimization or closed-loop feedback control. After printing, AI converts wearable sensing signals into physiological, biochemical, behavioral, and functional information. Together, these stages connect material and process design with fabrication quality, device performance, and the interpretation of wearable sensing outputs. **Section 3.1** first clarifies how AI-assisted bioprinting contributes to wearable biosensor fabrication,

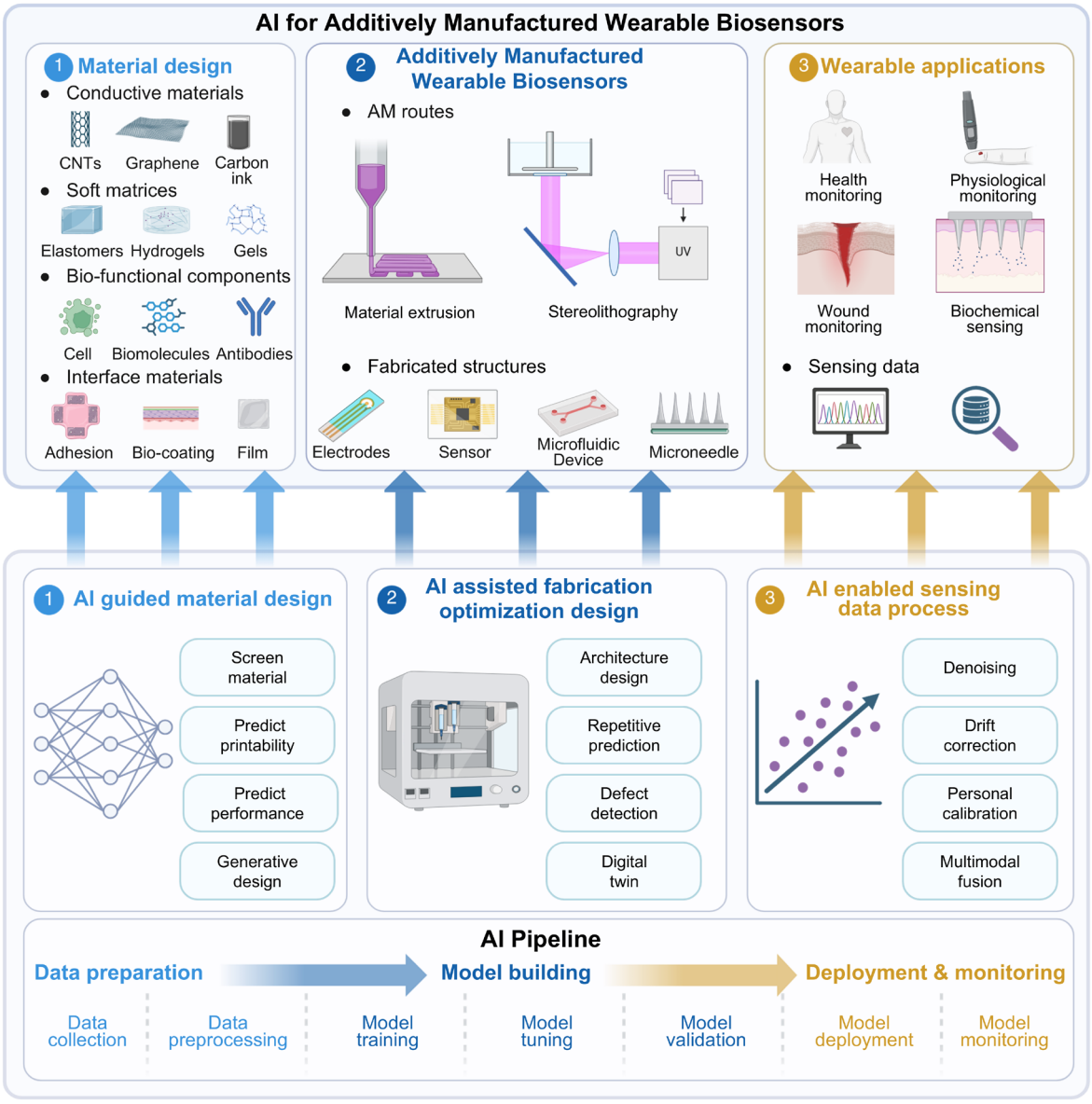


Figure 3. Three-stage AI workflow linking pre-printing design, in-process control, and post-printing applications in additively manufactured wearable biosensors
Abbreviations: AI: Artificial intelligence; AM: Additive manufacturing; CNT: Carbon nanotube.

sensor integration, and functional performance. **Sections 3.2–3.4** then examine the three stages, followed by a cross-stage comparison of the corresponding AI strategies in **section 3.5**.

3.1. Role of AI-assisted bioprinting

Wearable biosensors operate at a moving and deformable interface, so reliable performance depends on conformal contact and stable signal acquisition during use.[2,17,51] AM is attractive in this context because it can place functional materials within geometries tailored to the body.[2,31,47] In practice, each manufacturing step affects the next: formulation influences deposition, the deposited material defines the printed structure, and that structure shapes the sensing response.[46,47,56] As the design space expands, empirical adjustment becomes slow and offers limited insight into the interactions among these factors.[60,61] AI can learn these relationships from experimental data and guide material and process selection toward device-level targets.

Bioprinting provides practical strategies for addressing this problem because it routinely handles soft functional inks whose properties evolve during printing.[46,47] AI models developed in this field have shown that formulation and rheology can be used to anticipate printability and define suitable processing windows.[60,61,65] This is directly relevant to wearable sensors based on conductive or biofunctional hydrogels, where successful deposition and functional performance after printing are closely linked.[31,47] For bioactive components, biological response can be included as a post-print functional outcome in the same material and process model. More broadly, this shows how AI-assisted formulation can account for the function retained after printing, including the sensing response required in wearable devices.

Bioprinting methods are also relevant to sensor integration. Wearable sensing features are often deposited on surfaces that curve or move.[37,67] Accurate placement and stable interfaces are therefore important during fabrication and subsequent deformation. Vision-based systems developed for extrusion bioprinting can recognize changes in filament formation and use feedback control to correct deposition during printing.[14,118] Deformation-aware printing further shows how deposition can follow a changing surface.[37,67] Together, these approaches offer practical routes to maintaining the continuity of printed sensing features on deformable platforms.

Process quality carries through to the measured signal. Changes in printed features or interfaces can alter the pathways through which the device converts physiological or biochemical inputs into measurable signals.[17,44,73] AI-assisted material design and process control can help trace these effects back to the conditions under which the device was printed. Evaluation should therefore connect print quality with sensing behavior under deformation and realistic wearing conditions.[51] Accordingly, this review draws on the bioprinting literature for transferable AI-assisted strategies that address wearable biosensor fabrication, integration, and performance. The following sections organize these strategies across pre-printing design, in-process monitoring and control, and post-printing analysis and applications.

3.2. AI-assisted pre-printing design

3.2.1. Data-driven design

As the first stage of the AI-assisted workflow, pre-printing design uses AI to guide material formulation, printability prediction, and initial process-window selection before fabrication (Table 4). This stage is especially important for AM-fabricated wearable biosensors because a printable material must also remain soft, conductive, biocompatible, and functionally active. These coupled requirements connect pre-printing design with advances in bioink design, hydrogel printing, bioprinting, and light-based printing, where formulation, printability, biological compatibility, and structural fidelity are often evaluated before fabrication.[13,119,120] A first group of studies used measurable material descriptors to predict printing outcomes before printing.

Lee *et al.*[60] provided one of the representative examples by linking bioink mechanical properties with 3D printability (Figure 4A). Their work showed that elastic modulus and yield stress are key descriptors for printable bioinks, where elastic modulus influences shape fidelity and yield stress governs extrusion feasibility. This descriptor-based strategy is useful for AM wearable biosensors because hydrogel interfaces, conductive hydrogels, elastomeric inks, and biofunctional inks all require material selection before device printing.[1,121] The broader importance of such early-stage material properties is also supported by da Silva *et al.*,[65] who showed that rheological, printability, swelling, and degradation characteristics can be used to predict later biological outcomes in fibrin-alginate-based neural bioinks (Figure 4B(i)–(iii)). In their study, support vector regression provided the most consistent overall trade-off across outputs and was the best-performing model in 83% of the analyzed features. These studies establish the first level of pre-printing design, where printable and functional materials are selected according to measurable mechanical, rheological, and biological parameters rather than empirical formulation trials.

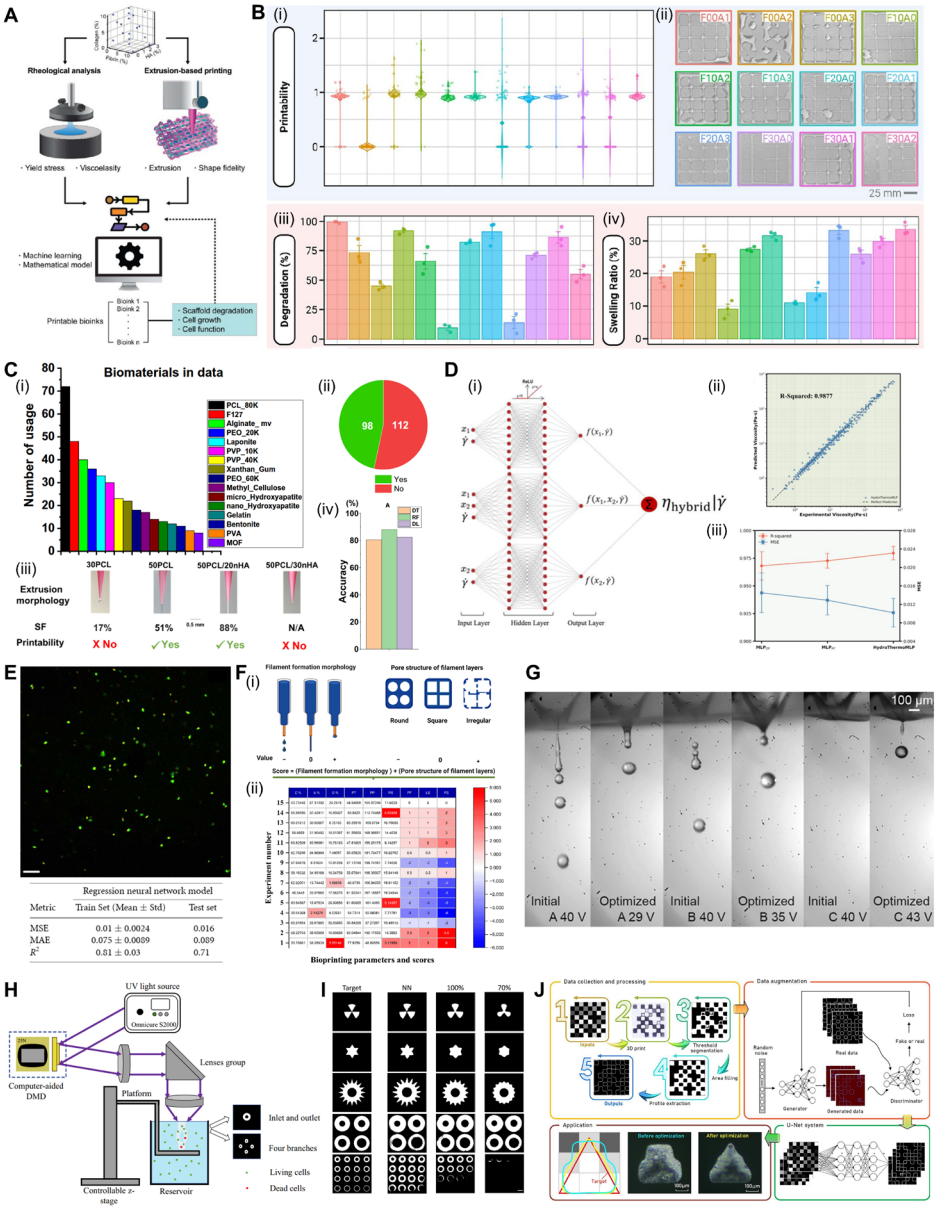


Figure 4. Data-driven AI-assisted pre-printing design for additively manufactured wearable biosensors. (A) Scheme of bioink development based on a mathematical model for predictive tissue engineering. Reprinted with permission from Lee *et al.*[60] Copyright © 2020 IOP Publishing. (B) Evaluation of testing bioink formulations. (i) Printability index. (ii) Representative printed structures. (iii) Degradation behavior after incubation. (iv) Swelling ratio after hydration.[65] (C) ML based prediction of biomaterial ink printability. (i) Distribution of biomaterials used in the dataset. (ii) Distribution of printability outputs. (iii) Representative printing outcomes of selected inks. (iv) Prediction accuracy of optimized ML models. Reprinted with permission from Chen *et al.*[61] Copyright © 2023 American Association for the Advancement of Science. (D) HydroThermoMLP model for hydrogel rheological property prediction. (i) Model framework. (ii) Fitting ability. (iii) Generalization performance. Reprinted with permission from Deng *et al.*[125] Copyright © 2025 Elsevier. (E) Regression neural network based prediction of hydrogel bioprinting outcomes, with live and dead fluorescence images and model performance metrics.[22] (F) Bayesian optimization based evaluation of bioink printability. (i) Scoring criteria for filament formation and layer stacking. (ii) Heatmap of printability scores under different formulation and printing parameters. Reprinted with permission from Hashemi *et al.*[64] Copyright © 2024 Elsevier. (G) Printing results of different bioinks using voltages optimized by multi objective optimization. Reprinted with permission from Shi *et al.*[24] Copyright © 2019 China Engineering Science Press. (H) Stereolithography-based bioprinting setup for ML-guided pattern optimization. Reprinted with permission from Xu *et al.*[37] Copyright © 2020 Springer Nature. (I) Postprocessed microscopic images of test prints. Columns 1 to 4 show target structures, prints generated using masks calculated by neural networks, and prints obtained with the same masks under 100% and 70% exposure doses, respectively. Scale bar: 200 μm. Reprinted with permission from Guan *et al.*[36] Copyright © 2021 IOP Publishing. (J) ML-assisted workflow for grayscale vat photopolymerization printing, including data collection, image processing, data augmentation, U-Net based profile prediction, and printing optimization.[35]
Abbreviations: AI: Artificial intelligence; ML: Machine learning.

Following this descriptor-level understanding, later work began to treat formulation design as a classification problem. Chen *et al.*[61] constructed a DIW dataset containing 210 biomaterial formulations prepared from 16 biomaterials and 4 solvents (Figure 4C(i)–(iii)). Instead of only relying on experimental screening, they trained DT, RF, and DL models to classify each formulation as printable or non-printable. The RF model achieved the best overall performance, with 88.1% accuracy, 90.6% precision, and an F1 score of 87.0%, while the DL model reached the highest recall of 87.3% (Figure 4C(iv)). More importantly, the trained models were used to generate printability windows for F127/Laponite hydrogel nanocomposites and PCL/nano-hydroxyapatite polymer nanocomposite inks. This work marks a transition from descriptor identification to formulation-space prediction, allowing printable windows to be mapped before experimental ink development.[121]

Besides classifying formulations, ML has also been used to explain why certain formulations become printable.[82,122] Nadernezhad and Groll[82] addressed this question using an interpretable ML framework for hydrogel formulations containing rheology additives. Based on 180 formulations, they identified 13 critical rheological measures associated with hydrogel printability. Its main contribution is interpretability, because the model explains which rheological measurements control printability instead of only assigning a printable or non-printable label. This is particularly useful when functional additives alter both sensing properties and extrusion behavior.[1,122,123]

A related direction is the direct prediction of rheological properties before printing. Sarah *et al.*[124] developed ML models to predict the viscosity of hybrid hydrogel bioinks composed of alginate, gelatin, and TEMPO-nanofibrillated cellulose over shear rates from 0.1 to 100 s^{-1}. Polynomial fit, DT, and RF models were compared using R^2 and MAE. The RF model performed best, reaching $R^2 = 0.99$ and MAE = 0.09, compared with $R^2 = 0.95$ and MAE = 0.28 for polynomial fit and $R^2 = 0.98$ and MAE = 0.13 for DT. Deng *et al.*[125] further extended rheology prediction to HAMA/GelMA hybrid hydrogels by comparing MLP, XGBoost, RF, and support vector regression, and then incorporating the Redlich–Kister polynomial into a HydroThermoMLP model (Figure 4D(i)–(iii)). These studies broaden pre-printing design from final printability prediction to intermediate property prediction, where viscosity and shear stress serve as measurable bridges between formulation and printed structure.

Once printable formulations are identified, the next pre-printing problem is selecting the initial processing window. Etefagh and Razfar[21] applied Bayesian optimization to 3D bioprinting of PCL/MgO nanocomposite scaffolds. Their model examined the effects of air pressure, printing speed, and nozzle temperature on printability and print resolution. Instead of exhaustively testing a broad parameter space, the Bayesian optimization framework identified suitable printing conditions within 11 iterations for each target filament width, and the predicted and measured filament widths showed 91% agreement. This study demonstrates how AI-assisted optimization can convert process-window selection into a data-efficient search problem, where printable resolution and structural accuracy are optimized before fabrication.

In a similar direction, Rane *et al.*[126] used surrogate-assisted multi-objective Bayesian optimization for bioink rheological design. Their Gaussian process-based framework optimized flow-property variables, including minimum viscosity, maximum viscosity, consistency index, flow behavior index, and nozzle outlet diameter, to reduce hydrodynamic shear stress during extrusion. After an initial set of 24 experimental runs, the sequential design required 21 iterations to converge toward Pareto-optimal flow properties. This study highlights the multi-objective nature of pre-printing design, where improved shape fidelity, reduced shear stress, and biological compatibility must be optimized together rather than independently.

Beyond printability and rheology, pre-printing ML can also consider biological performance. Mohammadrezaei *et al.*[22] developed neural network models to predict cell viability in extrusion-based bioprinting using a dataset of 591 instances generated from in-house experiments and literature data (Figure 4E). Their model incorporated bioink formulation, printing parameters, crosslinking conditions, cell type, and measurement time. The regression neural network achieved $R^2 = 0.71$, while the classification neural network reached an accuracy of 0.86. The study further integrated the regression neural network with Bayesian optimization to identify printing and crosslinking conditions that maximize cell viability. This work extends pre-printing design from structural printability to biological viability, which is important for biofunctional hydrogels, enzyme-loaded matrices, living interfaces, and wound-related sensing materials.[63]

Other work has similarly treated bioink composition and biological response as coupled design targets. Hashemi *et al.*[64] used ML-assisted parameter suggestion to develop a chitosan-gelatin-agarose biomaterial ink for extrusion-based 3D bioprinting (Figure 4F(i) and 4F(ii)). The optimized formulation contained 27% agarose, 53% chitosan, and 20% gelatin, and was evaluated in terms of printability, rheological properties, hydrophilicity, degradability, and cell response. Qiao *et al.*[23] studied cryoprotective GelMA-based bioinks for extrusion

cryobioprinting, using 5% GelMA as the base bioink and ethylene glycol or glycerol as permeable cryoprotective agents, together with lactose, raffinose, or trehalose. Four ML models were compared, including multiple linear regression, DT, RF, and artificial neural network, with the predictive powers order of ANN > RF > DT > MLR. These studies show that AI-assisted formulation design can move beyond generic printability toward application-specific constraints such as degradation, hydration, storage stability, and post-thaw survival.[121,123]

The same pre-printing logic has also been applied to inkjet deposition. Shi *et al.*[24] proposed a multi-objective optimization (MOO) method for drop-on-demand bioprinting using fully connected neural networks (FCNN). Their framework aimed to suppress satellite droplet formation while reducing droplet diameter and increasing droplet speed (Figure 4G). After optimization, stable single-droplet printing was achieved, and droplet speed increased from 0.88 to 2.08 m s^{-1}. This example extends pre-printing optimization from filament-based extrusion to droplet-based deposition, where droplet speed, diameter, and satellite formation must be optimized as coupled objectives.

Aerosol jet printing (AJP) further extends droplet-based direct-write patterning to aerosol-focused material deposition for printed electronics and wearable sensing. Early work described AJP as a fully additive route for printed passive electronic components and functional circuits.[29] More recently, Sharma and Seiti[127] developed an ML-based framework for printability assessment and process-window selection in AJP of PEDOT:PSS-based 2D lines and 3D high-aspect-ratio microstructures. They compared RF, Gaussian process regression (GPR), SVM, Generalized additive model (GAM), and neural network (NN) models, with R^2 values above 0.9 for 2D line printing and around 0.7 for 3D structures. The study also showed that 3D AJP has a narrower process window than 2D AJP, with carrier gas flow requiring more than four times tighter control. For AM-fabricated wearable biosensors, this type of model can guide the printing of fine conductive traces, microelectrodes, and conformal sensing features before fabrication.

Electrohydrodynamic (EHD) printing provides another route for high-resolution droplet-based deposition through electric-field-assisted material delivery. Singh *et al.*[107] used ridge regression, random forest regression, support vector regression, gradient boosting regression, and multilayer perceptron models to predict EHD spraying and drop-on-demand printing outputs, including droplet diameter, spray current, and ejection frequency. Using literature-extracted datasets across different EHD modes, gradient boosting regression achieved the best overall performance, with an average prediction error below 5%. This result is relevant to AM-fabricated wearable biosensors because EHD printing can pattern fine droplets, fibers, films, and nanostructures, while its process window depends on coupled ink properties, electric field, nozzle geometry, and flow conditions. A related study by Toptaş and Yılmaz [128] further showed that interpretable ML and SHAP analysis can help analyze nonlinear electro-fluidic behavior in EHD systems.

Apart from material and parameter selection, high-throughput screening has provided another way to accelerate pre-printing optimization. Chen *et al.*[16] developed an AI-assisted high-throughput printing-condition-screening system for hydrogel architectures. The system combined a programmable pneumatic extrusion printer with AI-assisted image analysis to screen printing pressure, moving speed, and nozzle-to-substrate distance. It then generated phase diagrams describing extruded pattern morphology and line uniformity. Optimized alginate-gelatin hydrogel scaffolds showed improved structural uniformity and were further evaluated for mechanical properties, biological performance, and diabetic wound healing. This study represents a system-level form of AI-assisted pre-printing design, in which automated printing and image-based analysis are combined to generate process maps before device fabrication.

While deposition-based printing mainly involves formulation, rheology, extrusion, and droplet stability, photopolymerization-based printing introduces a different pre-printing design problem.[129] Here, the critical variables include resin formulation, photoinitiator content, UV intensity, exposure time, layer thickness, light scattering, curing depth, and biological compatibility.[33] Xu *et al.*[37] developed an ensemble learning model to predict cell viability in dynamic optical projection stereolithography-based bioprinting (Figure 4H). The model used UV intensity, UV exposure time, GelMA concentration, and layer thickness as inputs. A full factorial design produced 81 conditions, each repeated five times, resulting in 405 data points. When 10% of the dataset was used for testing, the ensemble model achieved R^2 = 0.953, RE = 0.013, and RMSE = 0.015. Feature-importance analysis showed that UV exposure time was the most significant variable, followed by layer thickness, GelMA concentration, and UV intensity. This study shows that photopolymerization-based pre-printing design must account for both curing conditions and biological damage, especially when light exposure directly affects cell viability or bioactivity.

In light-based printing, another important challenge is optical distortion caused by scattering. Guan *et al.*[36] used

Table 4. Representative AI studies relevant to pre-printing design for additively manufactured wearable biosensors.

AM method	Material	Printing output	AI target	AI model	AI outcome/metrics	Year & Ref.
DIW	Collagen-based bioinks	Printability, shape fidelity	Descriptor identification	ML-supported regression	Elastic modulus and yield stress identified	2020,[60]
DIW	F127/Laponite, PCL/nHA inks	Printable windows	Printability classification	DT, RF, DL	RF accuracy 88.1%, precision 90.6%, F1 87.0%	2023,[61]
DIW	HA-based hydrogels with rheology additives	Hydrogel printability	Rheology-printability interpretation	Interpretable ML	180 formulations, 13 rheological descriptors	2022,[82]
DIW	Alginate/gelatin/ TEMPO-NFC hydrogels	Viscosity	Viscosity prediction	PF, DT, RF	R^2 = 0.99, MAE = 0.09	2025,[124]
DIW	Fibrin-alginate neural bioinks	Bioink performance	Biological outcome prediction	SVR, linear models	SVR best in 83% of features	2026,[65]
DIW	PCL/MgO nanocomposite scaffolds	Filament width, print resolution	Process-window optimization	Bayesian optimization	11 iterations, 91% agreement	2021,[21]
DIW	Gelatin-alginate bioinks	Cell viability	Viability prediction	Neural network	R^2 = 0.71, accuracy = 0.86	2024,[22]
DIW	Chitosan/gelatin/ agarose bioink	Printability, cell response	Bioink formulation optimization	Bayesian optimization	27% agarose, 53% chitosan, 20% gelatin	2024,[64]
DIW	GelMA-based cryoprotective bioinks	Post-thaw cell viability	Bioink formulation prediction	MLR, DT, RF, ANN	ANN performed best	2023,[23]
Inkjet printing	Sodium alginate cell-laden bioinks	Droplet stability	Droplet optimization	FCNN, MOO	Speed 0.88 to 2.08 m s^{-1}	2019,[24]
AJP	PEDOT:PSS-based inks	2D lines 3D microstructures	Process-window optimization	RF, GPR, SVM, GAM, NN	R^2 > 0.9 for 2D printing R^2 ≈ 0.7 for 3D printing	2025,[127]
EHD printing	Conductive functional inks	Droplet diameter, Ejection frequency	Process-output prediction	SVR, GBR, MLP	Average error <5%	2023,[107]
SLA	GelMA/LAP/3T3 fibroblast bioink	Cell viability	Viability prediction	Ensemble learning	R^2 = 0.953, RMSE = 0.015	2022,[37]
DMD	GelMA/LAP/C2C12 cell-laden bioink	Printing fidelity	Light-scattering compensation	DL	32 prints to 4000 pairs	2021,[36]
DMD	Commercial resins	Boundary fidelity	Grayscale boundary prediction	U-Net, CGAN	Deviation reduced 30%	2024,[35]
DLP	PEGDA/Irgacure 819/ Sudan I resins	Polymerization accuracy	Pixel light optimization	ROM, CNN	Oversizing reduced	2025,[34]

Abbreviations: AJP: Aerosol jet printing; ANN: Artificial neural network; CGAN: Conditional generative adversarial network; CNN: Convolutional neural network; DIW: Direct ink writing; DL: Deep learning; DLP: Digital light processing; DMD: Digital micromirror device; DT: Decision tree; EHD: Electrohydrodynamic; FCNN: Fully connected neural network; GAM: Generalized additive model; GBR: Gradient boosting regression; GelMA: Gelatin methacryloyl; GPR: Gaussian process regression; HA: Hyaluronic acid; MAE: Mean absolute error; ML: Machine learning; MLP: Multilayer perceptron; MLR: Multiple linear regression; MOO: Multi-objective optimization; NFC: Nanofibrillated cellulose; nHA: Nano-hydroxyapatite; NN: Neural network; PCL: Polycaprolactone; PEGDA: Poly(ethylene glycol) diacrylate; PF: Polynomial fit; RF: Random forest; ROM: Reduced-order model; RMSE: Root mean square error; SLA: Stereolithography; SVM: Support vector machine; SVR: Support vector regression.

DL to compensate for cell-induced light scattering in DLP-based bioprinting. Cell-laden bioinks scatter projected light, causing deviations between the digital mask and the printed structure. Their method learned from mask-structure image pairs and generated compensated digital masks (Figure 4I). A learning-based data augmentation strategy reduced the required training samples by 10-fold, with only 32 trial printings augmented to 4000 data pairs for neural network training. Unlike extrusion-based studies that optimize material flow, this work uses AI to correct the optical transfer from digital pattern to cured structure before printing.

More recent studies have moved from scattering compensation to pixel-level fidelity optimization. Ma *et al.*[35] improved vat photopolymerization fidelity using ML-driven boundary prediction for grayscale pixel design. Their approach used a chessboard-pattern data acquisition strategy, automated data refinement, and U-Net-based modeling to learn the relationship between projected grayscale patterns and cured structures (Figure 4J). The method reduced geometric deviation by around 30%. Poltue *et al.*[34] further developed an ML framework for optimizing pixel light intensities in DLP printing, using a reduced-order model to track the degree of conversion of photocuring in three-dimensional space and optimize light patterns for targeted shapes. These studies push pre-printing design toward pixel-level exposure engineering, where AI is used to pre-compensate geometric errors before they appear in the printed structure.

Taken together, AI-assisted pre-printing design has expanded from descriptor discovery and formulation screening to process-window search, biological-performance prediction, and light-pattern correction. In deposition-based printing, current AI studies mainly use ML models to guide material selection, rheology-based printability prediction, droplet optimization, and extrusion-parameter selection. In photopolymerization-based printing, ML and DL models are more often used to describe resin behavior, optimize exposure conditions, predict cell viability, compensate optical scattering, and improve geometric fidelity. These studies also point to AM routes that remain less developed for wearable biosensors. In screen printing, AI could help tune ink viscosity, particle loading, mesh size, squeegee speed, drying condition, and electrode uniformity. In embedded printing, AI could help coordinate ink rheology, support-bath behavior, nozzle motion, crosslinking, and channel fidelity. In 2PP, AI could support resin selection, voxel-scale exposure control, writing-path design, and micro- or nanoscale structural accuracy. Compared with DIW, inkjet printing, and SLA/DLP, however, these methods still have fewer studies that define explicit AI targets and report quantitative pre-printing metrics. At present, AI use in pre-printing design remains concentrated in formulation screening, extrusion-parameter optimization, and light-based fidelity correction, whereas several AM routes for wearable biosensors remain underexplored. For AM-fabricated wearable biosensors, pre-printing design is more than a material-screening step. It defines the initial material and process space that later determines printability, structural fidelity, softness, conductivity, biocompatibility, and sensing activity. AI is useful at this stage because it can link material composition, process settings, and expected functional outcomes before fabrication. By ranking candidate formulations and identifying feasible process windows, these models can reduce the number of material combinations and printing conditions that require experimental evaluation. High-throughput screening, surrogate modeling, and Bayesian optimization further concentrate experimental effort on promising candidates, shortening the progression from formulation design to targeted validation. Their practical value therefore lies in guiding experiments toward informative regions of the design space while preserving experimental confirmation as the final basis for material and process selection. AI-assisted pre-printing design thereby establishes a more efficient and reproducible foundation for fabrication and device performance in the later stages of the workflow.

3.2.2. Generative design

Generative design uses AI models to create possible design options before fabrication, rather than only evaluating predefined materials, geometries, or printing conditions (Table 5).[130] In AM-fabricated wearable biosensors, it belongs to the pre-printing design stage because it operates before experimental printing. It can generate candidate device layouts, printed morphologies, material distributions, and process windows under constraints such as printability, mechanical compliance, transport behavior, and sensing performance. These candidates can then be screened and refined before fabrication.

Generative adversarial network (GAN)–based models have been used to learn bioinspired structural patterns from images. Shen and Buehler[131] trained a GAN on leaf micrographs and generated a library of 1000 leaf-inspired unit cells. The generated structures covered a broad density range and were further processed, tiled, printed, and mechanically evaluated (Figure 5A). Fang *et al.*[132] used single-image generative adversarial network (SinGAN) to generate cuttlebone-like structures from limited image data. The model used a 512 × 512 pixel training image and generated 10 sets of images, with 50 samples in each set. Finite element analysis showed that some generated

structures had higher elastic constants than the original structure, with improvements up to 11.63% under the transversely isotropic assumption and 9.38% under the orthotropic assumption. These studies are not wearable biosensor studies directly, but they show a useful design route for porous electrodes, compliant substrates, and hierarchical sensing interfaces.

Diffusion models provide another route for structure generation and inverse design. Stable Diffusion has been used to generate three-dimensional nature-inspired architected materials from language cues, followed by voxel reconstruction, additive manufacturing, and mechanical assessment (Figure 5B).[133] Attention-based diffusion models have also been used to link target mechanical responses with candidate hierarchical microstructures.[134] In this study, 1445 simulated stress-strain curves were retained for model training and validation, and the forward prediction reached $R^2 = 0.96$ on the validation set. This is relevant to wearable biosensors because device geometry controls deformation, contact, pressure response, and mass transport. A target mechanical or sensing response could be used to guide the design of printable device architectures.

Generative models can also help screen printed morphology before experiments. In 3D bioprinting, a beta-conditional variational autoencoder generated deposition morphologies from ink properties and printing parameters.[135] The generated morphologies were evaluated by a multi-task convolutional neural network using five printability metrics, including filament continuity, filament width, construct area, Dice similarity coefficient, and Hausdorff distance (Figure 5C). The framework further coupled the b-CVAE image generator with support vector regression, Bayesian optimization, and CNN-based printability evaluation. This workflow is useful for AM wearable biosensors because hydrogels, conductive inks, elastomers, and biofunctional inks often have narrow printable windows. Virtual morphology screening can reduce trial-and-error experiments before fabrication.

Large language models (LLMs) and vision-language models (VLMs) support generative design in a different way. BioinspiredLLM was trained on biological and bioinspired materials literature and used for knowledge recall, hypothesis generation, and research assistance.[136] In a 100-question biological materials exam, BioinspiredLLM achieved a baseline score of 82%, which increased to about 90% after adding step-by-step prompting (Figure 5D). Cephalo combined image and text inputs for bioinspired materials analysis and design.[137] After fine-tuning with molecular dynamics data, Cephalo predicted stress-distribution statistics with R^2 values of 0.98, 0.95, and 0.92 for standard deviation, mean, and median stress,

Table 5. Representative generative AI studies relevant to pre-printing design of additively manufactured wearable biosensors

Generative AI model	Generation method	Generated output	Reported result	Year & Ref.
GAN	Image-based structure generation from leaf micrographs	Leaf-inspired 2D and 3D architectures	1000 unit cells; printed and tested	2022,[131]
SinGAN	Single-image generation from cuttlebone images	Cuttlebone-like biomimetic structures	Elastic constant +11.63%	2023,[132]
Diffusion model	Text-to-image generation and 3D reconstruction	Nature-inspired 3D architected materials	Printed and mechanically assessed	2022,[133]
Attention-diffusion	Target-response-guided inverse design	Hierarchical microstructures	$R^2 = 0.96$	2023,[134]
b-CVAE	Condition-guided image generation from ink and process inputs	Deposition morphologies	BO-CNN printability screening	2026,[135]
LLM	Text generation from literature and prompts	Design hypotheses and research suggestions	Exam score up to ~90%	2024,[136]
LLM	Knowledge-graph reasoning	Research hypotheses	Novelty/feasibility scoring	2025,[138]
VLM	Image-text reasoning from figures and prompts	Structure interpretation and design guidance	R^2 up to 0.98; crack-detection accuracy 0.98	2024,[137]

Abbreviations: b-CVAE: Beta-conditional variational autoencoder; BO-CNN: Bayesian optimization–convolutional neural network; GAN: Generative adversarial network; LLM: Large language model; SinGAN: Single-image generative adversarial network; VLM: Vision-language model.

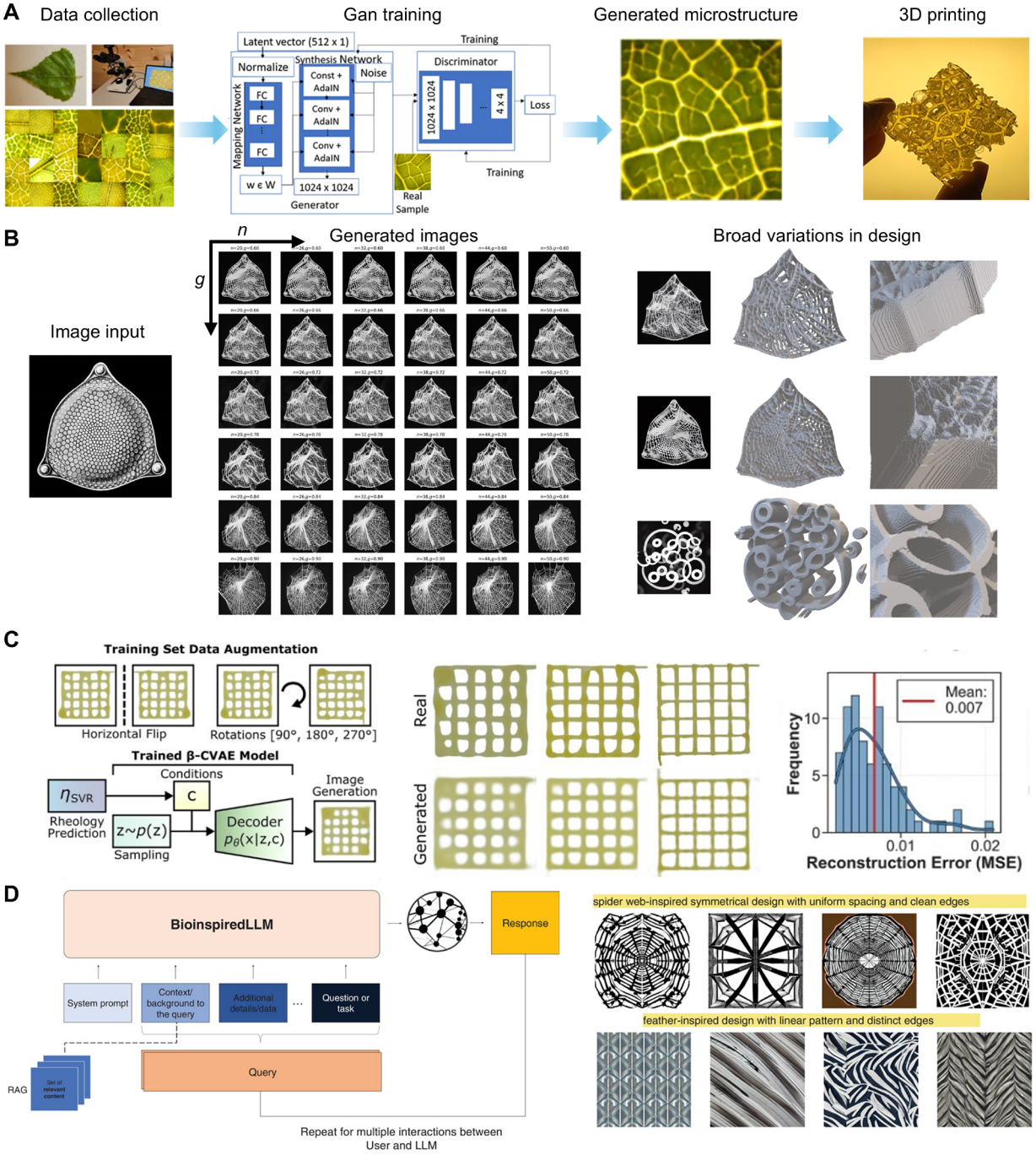


Figure 5. Generative AI approaches for pre-printing design in additively manufactured wearable biosensors. (A) Overview of leaf image generation, dataset construction, and manufacturing. A GAN was trained using leaf images to generate continuously varying microstructures in latent space. Selected structures were converted into 3D models and fabricated by stereolithography.[131] (B) Diffusion-model-based image generation from a single image input. The generated images provide structure candidates that can be further converted into 3D architectures for additive manufacturing and mechanical assessment.[133] (C) Beta-conditional variational autoencoder for generating grid-structure images in 3D bioprinting. The panel shows the generated printing results and the distribution of mean squared error (MSE) for the test set.[135] (D) BioinspiredLLM workflow based on graph-forming attention mechanisms from system prompts and user queries to generated responses. Three prompts suggested by BioinspiredLLM were used as inputs for Stable Diffusion 2.0. Each prompt generated four image outputs, and one selected image was processed into a 3D model for visualization, simulation, or experimental feedback.[136]

Abbreviations: AI: Artificial intelligence; GAN: Generative adversarial network.

respectively. It also predicted atomic potential energy statistics with R^2 values of 0.97, 0.96, and 0.95, and reached 0.98 accuracy, precision, recall, and F1 score for crack-initiation classification. These models do not directly validate wearable device performance. Their value is in connecting literature, figures, material features, and design constraints during early-stage design.

Generative design adds a candidate-generation step to the pre-printing design of AM-fabricated wearable biosensors. It learns from existing material, structure, and process data, then produces multiple possible designs under defined constraints. This step is useful because wearable biosensors often require coupled optimization of geometry, material distribution, and interface function. The generated candidates can expand the design space for later printability screening, performance testing, and wearable validation.

3.3. AI-assisted in-process monitoring and control

As the second stage of the AI-assisted workflow, in-process control focuses on printing stability, defect management, and parameter regulation during fabrication (Table 6).[139] In this stage, open-loop AI systems optimize printing conditions without real-time feedback correction. These methods use prior experimental data, process models, or offline measurements to predict printing outcomes, detect likely defects, recommend process parameters, and improve printed structure quality. Although they do not adjust the process during printing in real time, open-loop AI frameworks can reduce trial-and-error experiments and improve printing fidelity, process efficiency, and reproducibility across different AM technologies.

Jin *et al.*[78] developed a DL-based anomaly detection framework for extrusion bioprinting using convolutional neural networks (CNNs) combined with image augmentation techniques to identify defects in transparent hydrogel structures (Figure 6A(i)). The framework analyzed layer-by-layer sensor images and classified defects such as discontinuous filaments, irregular line widths, and bubble formation during hydrogel printing. CNN-based image recognition enabled simultaneous localization and classification of defects together with identification of infill patterns (Figure 6A(ii)). The study demonstrated high anomaly detection accuracy and significantly improved monitoring efficiency compared with manual post-print inspection (Figure 6A(iii)). By rapidly identifying fabrication imperfections, the proposed framework reduced material waste and improved dimensional fidelity in hydrogel-based bioprinting applications, providing a foundation for future autonomous manufacturing systems with intelligent defect monitoring capabilities. Dabbagh *et al.*[81] integrated ML with extrusion-based 3D printing through a graphical user interface (GUI) designed to optimize process parameters and predict printing quality. The framework evaluated nine CAD geometries and introduced a complexity index capable of quantifying geometric difficulty during printing. Four labeling strategies were developed to compare printed structures with target CAD models. Eight ML algorithms were trained on a dataset of 224 datapoints, with gradient boosting regression achieving the best predictive performance at an R^2 value of 0.954. The developed GUI enabled users to upload designs and predict printing similarity under selected process conditions before fabrication. The framework substantially reduced trial-and-error optimization, shortened design-to-manufacturing time, minimized material waste, and improved geometric fidelity in extrusion-based additive manufacturing processes. Rezapour Sarabi *et al.*[140] developed an ML-enabled framework for predicting and evaluating the quality of 3D-printed microneedle arrays fabricated using FDM followed by chemical etching. DL methods were employed for quality control and anomaly detection in printed microneedle arrays using image-based datasets generated from ten different microneedle geometries and multiple etching conditions. ML algorithms extracted similarity metrics capable of predicting fabrication outcomes under different process parameters. The framework enabled automated evaluation of microneedle geometry and structural fidelity while reducing manual inspection requirements. By integrating AI-assisted prediction with microneedle fabrication, the study improved manufacturing efficiency, enabled rapid parameter optimization, and accelerated the development of high-precision biomedical microneedle systems for transdermal drug delivery and biosensing applications.

Fu *et al.*[71] investigated the effects of extrusion bioprinting parameters on the printability of Pluronic F127 hydrogels and developed an SVM-based ML framework for process optimization. The study evaluated the influence of rheological properties, nozzle gauge, nozzle temperature, path height, and ink composition on print quality and dimensional fidelity. Experimental datasets were used to generate process maps capable of identifying optimal printing conditions with a probability exceeding 75% for producing high-quality structures. The SVM framework effectively reduced the number of experimental trials required for process optimization while improving printing reproducibility and dimensional accuracy. The study demonstrated that ML-assisted parameter selection provides an efficient approach for improving extrusion bioprinting reliability and printability in hydrogel-based additive manufacturing systems. Ruberu *et al.*[141] coupled Bayesian optimization

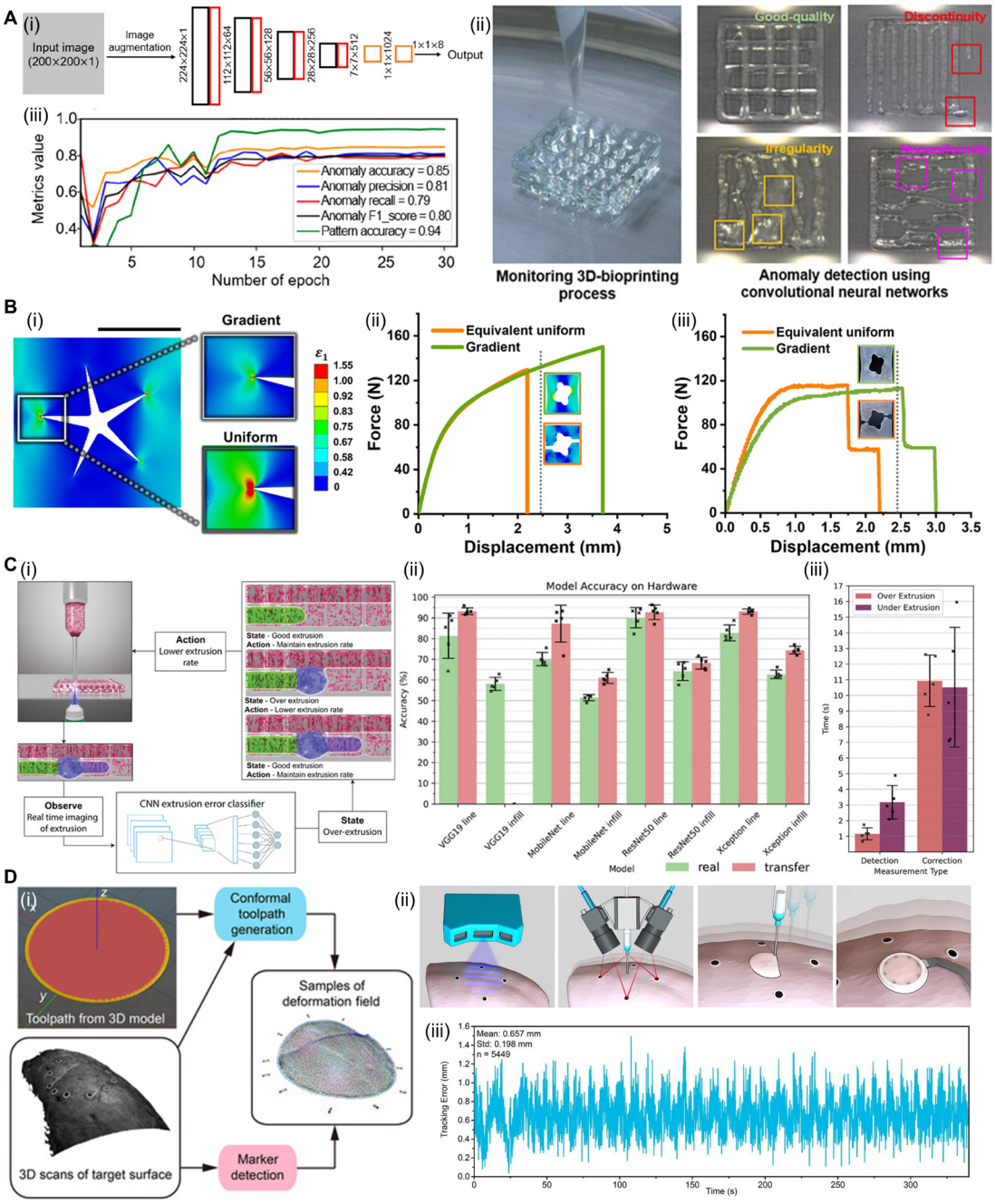


Figure 6. AI-assisted open-loop monitoring and closed-loop control in additive manufacturing. (A) CNN-based anomaly detection in extrusion bioprinting. (i) Open-loop flow diagram of the CNN model. (ii) 3D bioprinting process with anomaly detection using CNN. (iii) Model performance over 30 training epochs evaluated on the validation dataset. Reprinted with permission from Jin *et al.*[78] Copyright © 2023 ACS Publishing. (B) AI-guided grayscale DLP printing for programmable mechanical response. (i) Finite element strain distributions of structures printed with uniform and gradient grayscale exposure. (ii). FEA-predicted force-displacement curves of DLP-printed structures with uniform and gradient grayscale intensities. (iii). Experimental force–displacement responses of DLP-printed structures fabricated using uniform and gradient grayscale intensities.[38] (C) Closed-loop extrusion error detection and correction. (i) CNN-based framework for detecting over-extrusion and under-extrusion during extrusion bioprinting. (ii) Model accuracy on hardware. (iii) Detection and correction times for single-line printing. Reprinted with permission from Kelly *et al.*[14] Copyright © 2025 John Wiley and Sons. (D) Closed-loop conformal printing on moving biological surfaces. (i) Toolpath generation from 3D surface scanning and marker detection. (ii) *In situ* printing of a sensor on a dynamically breathing lung surface. (iii) Real-time tracking error during printing. Reprinted with permission from Zhu *et al.*[67] Copyright © 2020 American Association for the Advancement of Science.

Abbreviations: AI: Artificial intelligence; CNN: Convolutional neural network; DLP: Digital light processing; FEA: Finite element analysis.

with extrusion bioprinting to quantitatively evaluate printability and accelerate optimization of GelMA and hyaluronic acid methacrylate (HAMA) bioinks. A scoring system incorporating filament formation and scaffold layer stacking performance was established to quantify printability during fabrication. Bayesian optimization identified optimal printing parameters for multiple hydrogel formulations while dramatically reducing the experimental search space. For GelMA inks, optimal conditions were identified within 4–47 experiments, whereas GelMA:HAMA formulations required only 25–32 experiments compared with approximately 6000–10,000 possible parameter combinations. The ML-assisted optimization framework significantly reduced material consumption and experimental workload while improving scaffold reproducibility and printing consistency. The study demonstrated that open-loop AI optimization can efficiently predict processing conditions and improve fabrication performance in extrusion-based bioprinting applications. Bone *et al.*[142] proposed a hierarchical ML framework to optimize printability and dimensional fidelity in extrusion-based bioprinting of alginate hydrogels fabricated using freeform reversible embedding of suspended hydrogels (FRESH). The study systematically varied process parameters including print speed, flow rate, nozzle diameter, and ink concentration to generate 48 experimental datasets for model training. Least absolute shrinkage and selection operator (LASSO) regression was used to identify dominant variables influencing print error, while a parameterized middle-layer model improved prediction capability between process parameters and print fidelity. The optimized HML framework achieved an R^2 value of 0.643 between predicted and observed print quality. High-fidelity structures were defined as prints exhibiting less than 10% dimensional error relative to CAD geometry. The ML framework successfully generated predictive process maps that minimized experimental iterations and improved printability optimization for hydrogel bioprinting applications.

Nam *et al.*[38] proposed an ML-driven grayscale digital light processing (g-DLP) framework for fabricating mechanically robust gradient materials with programmable mechanical properties. The study combined polyurethane acrylate (PUA) resin synthesis with Bayesian multi-objective optimization to improve mechanical robustness and reduce strain concentration in printed structures (Figure 6B(i)–(iii)). The developed resin system expanded the achievable elastic modulus range from 8.3 MPa to 1.2 GPa while maintaining high damping performance. Bayesian optimization enabled identification of optimized gradient structures that reduced strain concentration by up to 83% and delayed crack initiation in mechanically stressed regions. The framework demonstrated the ability to optimize arbitrary three-dimensional geometries and significantly improve mechanical performance in gradient DLP-printed structures for applications including biomimetic cartilage and energy-absorbing systems. Maleki *et al.*[39] incorporated ML into the design and optimization of PLA-based bio-nanocomposites fabricated using DLP 3D printing. The study evaluated the effects of layer thickness, reinforcement type, and nanoparticle concentration on the mechanical and tribological properties of printed bio-nanocomposites reinforced with alumina, silica, and graphene nanoparticles. ML models were employed to predict tensile strength and wear resistance based on experimental datasets. Increasing alumina concentration to 8 wt.% improved tensile strength by approximately 16%, while graphene reinforcement enhanced wear resistance by 77%, outperforming silica (69%) and alumina (62%). The study demonstrated that ML-assisted optimization can effectively predict material performance and accelerate the development of mechanically enhanced DLP-printed biomedical nanocomposites.

Shetty *et al.*[25] developed an ANN-assisted optimization framework for 3D-printed PLA bone scaffolds using finite element analysis and Taguchi orthogonal array experimental design. Three lattice geometries, including gyroid, diamond, and lidinoid structures, were analyzed under compressive loads ranging from 3 to 9 kN with varying wall thicknesses. Among all configurations, the gyroid lattice demonstrated the best mechanical performance, exhibiting the lowest displacement of 0.36 mm and strain of 1.2×10^{-2} at 3 kN with 2 mm wall thickness. The back-propagation ANN model achieved extremely high predictive accuracy with R^2 values of 0.9991 for displacement prediction and 0.9954 for strain prediction. The study demonstrated that AI-assisted predictive modeling can accurately optimize scaffold geometry and mechanical behavior for bone tissue engineering applications.

Closed-loop AI-assisted printing systems integrate real-time sensing, CV, and adaptive control algorithms to continuously monitor fabrication quality and dynamically correct printing errors during manufacturing. These systems significantly improve dimensional fidelity, process stability, and printing reproducibility in additive manufacturing applications.

Arduengo *et al.*[118] developed a closed-loop extrusion bioprinting system incorporating real-time CV to dynamically control filament width during hydrogel extrusion. A camera-based monitoring system continuously measured the deposited filament immediately after extrusion and adjusted the extrusion feed rate in real time through feedback control. The

Table 6. Representative AI studies for in-process monitoring and control in additive manufacturing

Control strategy	AM method	Material	AI output	AI input	AI method	Ref.
Open-loop	DIW	Transparent hydrogel bioinks	Anomaly detection	Layer-by-layer sensor images	Deep neural networks	2023,[78]
	FDM	Biodegradable PLA	Anomaly detection	Printed microneedle images	SVM, CNNs, PaDiM	2022,[140]
	DIW	Multiple biomaterials	CAD-print similarity score	CAD complexity, temperature, and pressure	Gradient boosting	2022,[81]
	DIW	Pluronic F127 hydrogel	Quality classification	Material concentration, nozzle temperature, path height	SVM	2021,[71]
	DIW	GelMA and HAMA bioinks	Printability score	Material composition, temperature, pressure, speed	Bayesian optimization	2021,[141]
	DIW	Alginate hydrogels	Print fidelity score	Flow rate, nozzle speed, Alginate concentration, and nozzle diameter	Hierarchical ML, LASSO	2020,[142]
	DIW	Polyethylene glycol diacrylate	Printability score	Extrusion speed, temperature	Decision tree classifier	2025,[143]
	DLP	PUSA-HUA resins	Mechanical robustness	Gradient structure parameters	Bayesian optimization	2025,[38]
	DLP	PLA and nanoparticles	mechanical strength and wear resistance	Layer thickness, nanoparticle type and concentration	ANN	2025,[39]
	FDM	PLA	Displacement and strain prediction	Lattice geometry, wall thickness	ANN	2025,[25]
	DIW	Gelatin bioinks	Cell viability, filament diameter, extrusion pressure	Nozzle diameter, material concentration, temperature, pressure	RF regression/classification	2021,[72]
	DIW	Alginate bioinks	Cell viability	crosslinking parameter	NN, Bayesian optimization	2024,[22]
	2PP	IP-DIP photoresist	Part-quality classification	*In situ* TPL process video frames	Seq CNN-LSTM	2020,[115]
Closed-loop	DIW	Pluronic hydrogel	Line width	Real-time camera images	CV control	2025,[118]
	DIW	Alginate inks Pluronic ink	Extrusion quality class	Real-time camera images	Xception, ResNet	2025,[14]
	DIW	Conductive ink	Toolpath adaptation	Real-time geometric	CV control	2018,[66]
	DIW	Ionic hydrogel ink	Surface motion estimation	Real-time geometric	CV control	2020,[67]
	DIW	Microgel-based ink	Surface motion estimation	Real-time geometric	CV control	2024,[68]
	Volumetric 3D printing	Cell-laden bioresins	Adaptive channels, aligned overprints	Light-sheet images, 3D features	CV control, parametric modeling	2025,[117]

Abbreviations: 2PP: Two-photon polymerization; AI: Artificial intelligence; ANN: Artificial neural network; CAD: Computer-aided design; CNN: Convolutional neural network; CV: Computer vision; DIW: Direct ink writing; DLP: Digital light processing; FDM: Fused deposition modeling; LASSO: Least absolute shrinkage and selection operator; LSTM: Long short-term memory; ML: Machine learning; NN: Neural network; PaDiM: Patch Distribution Modeling; PLA: Polylactic acid; RF: Random forest; SVM: Support vector machine; TPL: Two-photon lithography.

framework was validated using Pluronic hydrogel across a wide range of line widths and rheological conditions. The closed-loop strategy significantly improved dimensional consistency and reduced variability caused by environmental fluctuations and bioink rheology changes. By maintaining stable filament deposition during printing, the framework improved reproducibility and enabled more reliable hydrogel bioprinting performance suitable for tissue engineering and biomedical manufacturing applications. Kelly *et al.*[14] proposed an autonomous extrusion bioprinting platform integrating CNNs with closed-loop feedback control for real-time error detection and correction (Figure 6C(i)–(iii)). Integrated cameras continuously monitored extrusion quality, while CNN architectures including Xception and ResNet classified extrusion states into good, over-extrusion, and under-extrusion categories. Transfer learning using synthetic and experimental datasets improved model robustness, with the Xception model achieving 90% classification accuracy for single-line extrusion and 75% accuracy for infill extrusion. The closed-loop control system dynamically corrected extrusion errors for alginate, collagen, and pluronic bioinks within approximately 10 s after defect detection. The framework substantially improved printing reliability, minimized process failures, and enhanced adaptability to materials with varying rheological properties during extrusion bioprinting.

Zhu *et al.*[66] developed a closed-loop adaptive 3D printing framework capable of fabricating functional materials directly onto moving freeform surfaces using real-time feedback control and dynamic toolpath adaptation. Stereo vision systems and deformation tracking algorithms continuously monitored target surface geometry and compensated for positional changes during printing. The framework enabled successful fabrication of functional and biological materials onto dynamically moving surfaces including skin and deformable tissues. In a subsequent study, Zhu *et al.*[67] later introduced a deformation-aware *in situ* printing framework for dynamically morphing organs such as breathing lungs (Figure 6D(i)–(iii)). Instead of assuming rigid motion, the system learned a low-dimensional deformation model using principal component analysis (PCA) from 3D scanned datasets and reconstructed conformal toolpaths from stereo-camera-tracked fiducial markers. The closed-loop AI system achieved submillimeter-scale deformation estimation accuracy while updating ≈3968 toolpath waypoints in real time to compensate for respiratory deformation during hydrogel sensor printing.

More recently, Jeong *et al.*[68] developed the INSIGHT system, which integrated an eye-in-hand depth camera with a 6-degree-of-freedom robotic arm to autonomously determine printing paths for irregular wounds and complex anatomical regions. Using OpenCV-based contour extraction, alpha-shape computational geometry, pointcloud reconstruction, and dynamic mesh generation, the system automatically generated adaptive printing trajectories from real-time wound geometry, depth, and color information. The closed-loop framework enabled continuous targeting of multiple wounds with >95% recognition accuracy while dynamically modifying extrusion and spray-printing paths to fabricate multimaterial constructs directly onto curved tissue surfaces.

Adaptive control has also been extended to volumetric printing. Florczak *et al.*[117] reported Generative, Adaptive, Context-Aware 3D Printing, which combines 3D imaging, computer vision, and parametric modeling to generate context-aware geometries for volumetric printing. In this workflow, light-sheet imaging maps features inside the printing volume, and the extracted spatial information is used to generate vessel-like channels, encapsulation structures, or sequentially aligned prints. The system completed scanning, feature isolation, model generation, and printing within about 4 min per spectral channel, while the alignment step took less than 5 s. Although GRACE is not a conventional real-time extrusion-control system, it extends closed-loop AI-assisted printing toward image-guided geometry generation, adaptive overprinting, and context-aware volumetric biofabrication. Together, these studies demonstrate that closed-loop AI not only improves extrusion stability but also enables intelligent, geometry-aware toolpath planning for adaptive manufacturing on dynamic biological surfaces.

AI-assisted in-process control improves AM fabrication by converting process data into predictions and corrective actions. Open-loop models can identify unstable conditions, prioritize suitable parameters, and estimate print quality before or during fabrication, thereby reducing experimental trials, failed prints, material waste, and repeated machine setup. Closed-loop systems extend this capability by combining real-time sensing with feedback control, allowing emerging defects to be detected and corrected during printing. This progression from offline prediction to active intervention improves dimensional fidelity, process stability, and manufacturing reproducibility while reducing operator-dependent variation. These capabilities are particularly important for biomedical and wearable devices that require reliable deposition on soft, curved, moving, or deformable surfaces. Practical implementation will require synchronized sensing, low-latency inference, reliable communication with machine

controllers, and validation across materials, printers, and operating conditions.

3.4. AI-assisted post-printing analysis and applications

As the third stage of the AI-assisted workflow, post-printing analysis uses AI to convert wearable sensing outputs into interpretable physiological and functional information after device fabrication and deployment. This stage is important for AM-fabricated wearable biosensors because these devices often generate time-dependent signals that are affected by body motion, skin contact, material deformation, environmental variation, and long-term device drift. Many printed wearable biosensors use soft, flexible, porous, or stretchable architectures to conform to irregular body surfaces and deform with the body during use. These structures improve wearing comfort, signal accessibility, and body-device integration, but they can also introduce nonlinear responses and motion artifacts. As a result, raw signals from AM-fabricated wearable biosensors are often difficult to interpret using simple calibration curves, fixed thresholds, or single-channel analysis. AI can address this problem by extracting features, correcting artifacts, identifying patterns, and linking raw electrical, optical, colorimetric, electrochemical, piezoresistive, or triboelectric signals with application-level outputs, including physiological-state prediction, motion recognition, gesture interpretation, voice recognition, symbolic communication, and tactile object identification (Table 7).

One important direction is the use of AI to interpret physiological, biochemical, or clinical-state information from 3D-printed wearable biosensors. For instance, Song *et al.*[17] developed a 3D-printed epifluidic electronic skin that integrated sweat biochemical sensing, physical sensing, soft microfluidics, and wearable electronics into a body-conformal platform (Figure 7A(i)–(iii)). The collected data included multimodal physiological and biochemical signals, and the authors used moving-average feature extraction with ridge regression to predict alcohol-related behavioral impairment indicators, including reaction time and commission error. This showed that AI improved the functional interpretation of the 3D-printed wearable system by linking multimodal sensor outputs to behavior-level outcomes rather than reporting individual signal traces alone. Similarly, Skonta *et al.*[144] developed 3D-printed PLA hollow microneedles loaded with chitosan nanoparticles containing glucose oxidase, horseradish peroxidase, and 2,2′-azino-bis(3-ethylbenzothiazoline-6-sulfonic acid) (ABTS) for colorimetric sweat glucose detection. In this case, smartphone photographs of the microneedle patches provided the colorimetric data, and the Random Sample Consensus algorithm was used to train a simple linear regression model for glucose prediction. The system achieved a glucose response range of 0.025–0.375 mM and a detection limit of 0.023 mM, showing that AI improved colorimetric biosensing by converting image-based color changes into quantitative biochemical readouts.

The same post-printing AI implementation logic has also been extended to wearable microneedle and electrophysiological platforms. Xie *et al.*[42] designed a wearable microneedle array colorimetric patch for interstitial-fluid sodium ions and uric acid monitoring (Figure 7B(i)–(iii)). The device used a vacuum-tube-driven microneedle array patch and a built-in colorimetric sensing paper, while self-designed CNN models were applied to reduce the influence of ambient light on colorimetric results and classify the sensing outcomes. This work demonstrated that AI improved the reliability of wearable colorimetric biosensing by compensating for practical imaging variations that would otherwise affect visual interpretation. Chen *et al.*[79] developed an AI-enhanced 3D-printed origami electrocardiogram (ECG) sensor for long-term cardiac monitoring (Figure 7C(i)–(iii)). The wearable ECG signals were transformed into scalogram images using continuous wavelet transform and then classified using a customized CNN. The system was used for real-time pre-diagnosis of sinus rhythm and ten atrial arrhythmia types and was demonstrated for continuous monitoring up to 34 h. This study showed that AI improved electrophysiological signal interpretation by converting raw ECG waveforms from a reusable 3D-printed dry electrode into diagnostic rhythm classification.

A second major post-printing application scenario is motion, gesture, gait, and user-intent recognition. In this group, AI is particularly useful because strain, pressure, capacitance, piezoelectric, and force-myography signals are highly time-dependent and often differ across users, motion amplitudes, and wearing positions. Qiu *et al.*[12] fabricated a printed liquid-metal sensory system by modifying liquid metal with SiO_2 particles to enable direct printing on soft materials, and integrated the resulting strain and pressure sensors into a tactile glove for boxing training (Figure 7D(i)–(iii)). The glove collected resistance-change signals during different punching motions, and a CNN-based deep-learning algorithm classified boxing techniques such as jab, swing, uppercut, and combination punches with 90.5% accuracy. In this case, AI improved the printed wearable sensor by translating coupled strain–pressure signals into sports-performance interpretation rather than only measuring deformation or impact strength. Hou *et al.*[145] developed multijet fusion (MJF) printed conformal strain and humidity sensors based on graphene

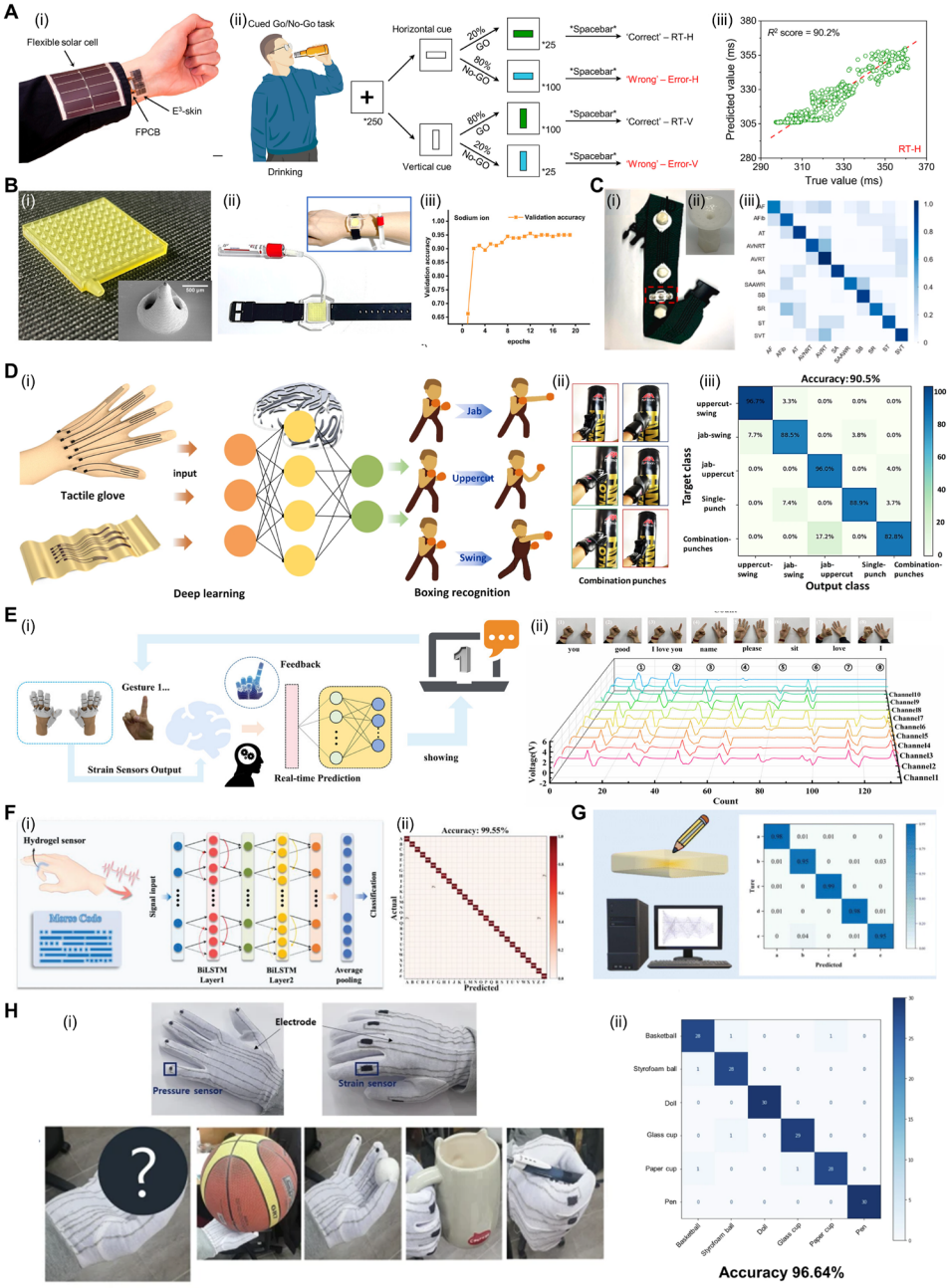


Figure 7. AI-enabled applications of additively manufactured wearable biosensors. (A) 3D-printed epifluidic electronic skin for multimodal health surveillance. (i) Wearable e^3-skin integrated with an FPCB and flexible solar cell. (ii) Cued Go/No-Go task for alcohol-related behavioral assessment. (iii) ML-predicted reaction time. Reprinted with permission from Song *et al.*[17] Copyright © 2023 American Association for the Advancement of Science. (B) Wearable microneedle colorimetric sensor. (i) Microneedle array. (ii) Wrist-mounted device. (iii) Training accuracy for sodium ion classification.[42] (C) 3D-printed origami ECG sensor for continuous cardiac monitoring. (i) Wearable ECG strip. (ii) Origami sensing unit. (iii) Confusion matrix for ECG classification. Reprinted with permission from Chen *et al.*[79] Copyright © 2026 Elsevier. (D) Liquid-metal tactile glove for boxing recognition. (i) Deep learning–assisted tactile sensing system. (ii) Representative punch classes. (iii) Classification confusion matrix.[12] (E) Smart glove for real-time gesture recognition. (i) Neural network–based gesture feedback system. (ii) Multichannel signals for common words.[15] (F) Wearable Morse-code recognition and translation system. (i) BiLSTM model. (ii) Confusion matrix for 26-letter recognition. Reprinted with permission from Zhuo *et al.*[26] Copyright © 2023 John Wiley and Sons. (G) TENG-based handwriting recognition and the confusion matrix of the classification task. Reprinted with permission from Chen *et al.*[40] Copyright © 2026 Elsevier. (H) Smart glove for tactile object recognition. (i) Printed tactile glove and tested objects. (ii) Confusion matrix for object classification.[27]

Abbreviations: AI: Artificial intelligence; BiLSTM: Bidirectional long short-term memory; ECG: Electrocardiogram; FPCB: Flexible printed circuit board; ML: Machine learning; TENG: Triboelectric nanogenerator.

nanoplatelet/carbon nanotube ink. They attached the sensors to body joints and used resistance-change signals from knee motion to train an SVM classifier, achieving 95.83% accuracy for six common motions, including walking, running, sitting down, squatting, jumping, and climbing stairs. The same device also monitored breath-related humidity signals. This showed that AI improved the printed conformal sensor by converting direction-dependent resistance changes into automated motion and respiration-state recognition.

Post-printing AI has also been used to infer user intent from wearable muscle-pressure or hand-motion signals. Young *et al.*[146] developed a gesture-recognition framework based on a soft pressure-based force-myography armband composed of 3D-printed pressure-sensitive chambers. The device collected upper-forearm peripheral force myography (pFMG) signals during hand gestures, and the framework included data acquisition, preprocessing, feature construction and selection, classifier selection, post-processing, and device actuation. The final system used a linear discriminant analysis (LDA)–based machine-learning workflow and achieved approximately 92.2% inter-session accuracy and 88.9% inter-trial accuracy for five gesture classes. This demonstrated that AI improved the 3D-printed pFMG armband by transforming muscle-derived pressure signals into user-intent commands for teleoperation of infrared consumer devices. Zhou *et al.*[147] directly 3D printed strain and pressure sensors onto a fabric glove using a conductive ink composed of multiwalled carbon nanotubes (MWCNTs), graphene nanosheets, fumed silica, and Ecoflex. They collected time-series resistance signals from five representative dynamic hand movements and used an LSTM neural network for gesture recognition and manipulator control. The LSTM model achieved 100% accuracy, showing that AI improved the smart glove by capturing temporal dependencies in dynamic gesture signals and enabling real-time robotic manipulation.

Other studies further show that AI can interpret more subtle or distributed body-movement signals. Zhang *et al.*[148] reported a 3D-printed self-powered piezoelectric sensor for gait recognition, where the wearable piezoelectric output was analyzed using a hybrid CNN-LSTM model. The CNN component extracted signal features while the LSTM captured temporal dependencies across gait cycles, leading to 98.7% accuracy for nine physiological postures and 93.7% accuracy for Parkinsonian gait-anomaly recognition. This shows that AI improved the self-powered printed wearable by converting piezoelectric signal sequences into gait-state and abnormal-motion classifications. Lin *et al.*[41] introduced MyoSpring, a wrist-worn mechanomyographic sensing system fabricated with customized 3D-printed springs. The mechanical signals generated by tendon and muscle deformation during subtle finger gestures were classified using an ML-based gesture-recognition workflow, achieving 94.11% average gesture accuracy and 91.44% accuracy for partial finger-flexion gestures. AI therefore improved the system by detecting fine motor intentions that are difficult to distinguish using threshold-based mechanical sensing alone. Truong *et al.*[149] developed a capacitive-sensing 3D-printed wristband that measured capacitance changes during hand gestures and used an RBF–SVM model for multiclass hand-gesture recognition. This study showed that AI improved indirect wrist-level sensing by mapping noisy capacitance changes into application-level hand commands, including game-control demonstrations. Together, these studies show that AI is particularly valuable when 3D-printed wearable biosensors are used to monitor motion, gesture, gait, and body movement, because the resulting sensor outputs are often nonlinear, time-dependent, and user-specific. Rather than treating printed wearable sensors as passive devices that only measure strain, pressure, capacitance, piezoelectric voltage, or force-myography signals, AI models such as CNN, SVM, LSTM, LDA, and hybrid CNN–LSTM frameworks enable the transformation of raw body-derived signals into interpretable behaviors, user intent, real-time commands, gait states, and functional performance indicators. In this sense, post-printing AI shifts 3D-printed wearable biosensors from mechanical or electrical signal acquisition toward behavior-level recognition and decision-support functions.

A third post-printing direction is semantic communication and symbolic-pattern recognition, where AI allows printed wearable sensors to move beyond motion detection toward language, voice, Morse-code, or handwritten-character interpretation. Lu *et al.*[15] developed an AI-enabled gesture-language-recognition feedback system by integrating silk-fibroin hydrogel strain-sensor arrays with a 3D-printed glove (Figure 7E(i) and 7E(ii)). The glove collected ten-channel resistance signals from finger motions, and a 1D-CNN model was used to classify 18 gesture-language patterns. The 1D-CNN achieved 99.333% accuracy, outperforming a visual geometry group (VGG)–based CNN model that achieved 93.222%. This showed that AI improved the 3D-printed smart glove by converting multichannel deformation signals into language-level gesture recognition and real-time feedback. Zhang *et al.*[150] developed a highly stretchable serpentine-shaped strain sensor using a 3D-printed TPU substrate and a conductive sensing layer. The sensors were integrated into a data glove, and an SVM classifier recognized ten common gestures with 96% accuracy and translated

them into audible speech. Here, AI improved the printed strain-sensor system by transforming hand deformation signals into communication-level outputs rather than only monitoring joint bending.

Voice, Morse-code, and handwritten-character recognition further demonstrate how AI can assign semantic meaning to printed wearable sensor signals. Liu *et al.*[151] developed topology-regulated 3D-printed polydimethylsiloxane (PDMS) foam piezoresistive sensors with conformal polydopamine/Ag interfaces and applied them to respiratory monitoring, insole-based gait analysis, and voice recognition. In the AI-assisted voice-recognition demonstration, the sensor was attached to the throat to collect vibration-induced resistance/current signals during pronunciation of Mandarin vowels, and an SVM model with cycle-wise feature extraction was used for vowel classification. The model showed strong recognition for several vowels, although lower performance was observed for acoustically similar vowels such as "u." This showed that AI improved the printed piezoresistive sensor by converting throat-vibration signals into voice-related behavioral interpretation. Zhuo *et al.*[26] fabricated Kirigami-inspired 3D-printable MXene organohydrogel strain sensors and integrated them with a bidirectional long short-term memory (BiLSTM) model for Morse-code recognition and speech translation (Figure 7F). The model processed resistance signals generated by finger-motion-based Morse-code gestures and achieved >99% recognition accuracy with a response time of approximately 17 ms, demonstrating that AI improved the wearable hydrogel sensor by enabling real-time symbolic communication.

Self-powered triboelectric nanogenerator (TENG)–based systems provide another route for AI-enabled symbolic interpretation because the sensor itself can generate voltage waveforms from mechanical contact. Chen *et al.*[40] developed a DLP 3D-printed microstructured ionic hydrogel electronic skin coupled with a hydrogel-based triboelectric nanogenerator (Figure 7G). For handwriting recognition, triboelectric voltage signals were segmented, standardized, converted into color images, and processed using a hybrid ResNet-18 + BiLSTM architecture. The model achieved 97% overall recognition accuracy and 96.8% cross-user validation accuracy, showing that AI improved the self-powered 3D-printed e-skin by converting handwriting-induced voltage signals into character-level information. Long *et al.*[152] developed a stretchable conductive hydrogel-based TENG and used a 1D-CNN model to classify voltage waveforms generated when numbers were written on the TENG surface. The model reached 99.11% recognition accuracy with a micro-average AUC of 0.99. Although this work is not primarily a 3D-printed wearable biosensor, it is useful as a supporting example because it shows how AI can interpret flexible TENG outputs as written-symbol information rather than simple contact or pressure responses.

A final application scenario is tactile object recognition, where AI is used to interpret distributed contact and grasping signals from printed wearable platforms. Pak *et al.*[27] developed a multifunctional wearable interconnect E-textile platform by DIW 3D printing strain sensors, pressure sensors, interconnect electrodes, and textile-integrated components directly onto fabric substrates (Figure 7H). The printed platform was used for body-motion monitoring, respiration tracking, and smart-glove tactile recognition. In the AI-assisted smart-glove demonstration, ten channels of resistance signals from printed strain and pressure sensors were collected during grasping of six objects, and RF and gradient boosting classifiers were used for object recognition. The models achieved 98.32% and 96.64% accuracy, respectively. This showed that AI improved the DIW-printed E-textile platform by converting multichannel mechanical sensing data into object-level tactile interpretation, allowing the system to identify what was being grasped rather than only reporting local strain or pressure.

Across these application scenarios, AI has been used more extensively for signal classification and motion recognition than for several reliability problems associated with continuous wearable monitoring. Motion, gesture, and gait recognition are well represented in the current literature, whereas the separation of physiological or biochemical signals from motion-induced interference remains less explored. Calibration across fabrication batches, devices, and users, together with signal drift and long-term operational stability, also requires further study. These gaps are particularly important because changes in printed geometry, skin contact, and operating conditions can alter sensor responses during practical use.

Taken together, these studies show that the practical contribution of post-printing AI lies in converting complex sensor responses into information that can support physiological monitoring, biochemical analysis, behavior recognition, communication, and human-machine interaction. Feature extraction, regression, illumination compensation, and pattern recognition extend the function of printed wearable biosensors beyond signal acquisition and enable electrical, optical, colorimetric, piezoresistive, and triboelectric responses to be interpreted at the application level. This capability is particularly valuable for soft and body-conformal devices, where nonlinear deformation, multimodal interactions, and user-dependent responses often limit the reliability of fixed

Table 7. Representative AI-enabled post-printing applications across wearable biosensing scenarios

Application scenario	AM method	Device	Signal	AI method	AI output/performance	Year & Ref.
Physiological and biochemical interpretation	DIW	Epifluidic e-skin	Sweat biochemical + physiological signals	Ridge regression	Health-state prediction	2023,[17]
	FDM	Microneedle	Smartphone colorimetric signal	RANSAC regression	Sweat glucose, LOD 0.023 mM	2025,[144]
	SLA	Microneedle colorimetric	ISF sodium and uric acid colorimetric signals	CNN	Light-resistant colorimetric classification	2025,[42]
	FDM	Origami ECG sensor	ECG waveform	CNN	Ten arrhythmia types, 34 h monitoring	2026,[79]
Body-motion recognition	DIW	Liquid-metal tactile glove	Strain/pressure resistance	CNN	Boxing recognition, 90.5% accuracy	2023,[12]
	MJF	Strain/humidity wearable sensor	Strain/humidity resistance	SVM	Motion prediction, 95.83% accuracy	2023,[145]
	DIW	Smart glove	Strain/pressure resistance	LSTM	Dynamic gesture recognition, 100% accuracy	2023,[147]
	DIW	Gait sensor/insole	Piezoelectric gait signal	CNN-LSTM	Posture 98.7%, gait anomaly 93.7%	2025,[148]
	SLA	MyoSpring bracelet	MMG signal	SVM	Finger gesture recognition, 94.11% accuracy	2022,[41]
Symbolic communication	DIW	Smart glove	10-channel resistance	1D CNN	Gesture-language recognition, 99.333% accuracy	2023,[15]
	FDM	Serpentine data glove	Resistance signal	SVM	Ten gestures, 96% accuracy	2024,[150]
	DIW	Throat/insole/respiratory sensor	Piezoresistive signal	SVM	Vowel and voice recognition	2026,[151]
	DIW	Kirigami organohydrogel sensor	Resistance signal	BiLSTM	Morse-code translation, >99% accuracy	2023,[26]
	DLP	Ionic hydrogel e-skin TENGs	Triboelectric voltage	ResNet-18 + BiLSTM	Handwriting recognition, 97% accuracy	2026,[40]
Tactile object recognition	DIW	E-textile smart glove	Strain/pressure resistance	RF, gradient boosting	Object recognition, 98.32% RF accuracy	2025,[27]

Abbreviations: AI: Artificial intelligence; AM: Additive manufacturing; BiLSTM: Bidirectional long short-term memory; CNN: Convolutional neural network; DIW: Direct ink writing; DLP: Digital light processing; ECG: Electrocardiogram; FDM: Fused deposition modeling; ISF: Interstitial fluid; LSTM: Long short-term memory; MJF: Multi Jet Fusion; MMG: Mechanomyography; RANSAC: Random Sample Consensus; RF: Random forest; SLA: Stereolithography; SVM: Support vector machine.

thresholds or simple calibration curves. Its practical value will depend on integrating signal-analysis models with printed device architecture, sensing mechanisms, body-interface mechanics, and real-world operating conditions.

3.5. Cross-stage comparison and algorithm selection

The studies reviewed across the three stages show that algorithm performance depends strongly on the learning task, input structure, dataset size, and validation strategy (Table 8). Within this task-dependent landscape, several consistent patterns emerge: ensemble and kernel-based models perform strongly on structured datasets with limited samples, CNNs excel in image-based analysis, and sequence-learning models are well suited to time-dependent sensing signals. These differences also shape the practical role of AI at each stage, from reducing experimental screening before printing to improving process robustness during fabrication and supporting reliable interpretation after deployment. Table 8 summarizes representative within-study comparisons and highlights the best-reported performance for specific tasks. The reported values are interpreted within their original experimental settings because materials, datasets, targets, and evaluation protocols vary among studies.

Pre-printing design typically begins with relatively small datasets composed of formulation variables, rheological properties, and processing descriptors. This data structure favors models that capture nonlinear interactions without requiring extensive training data. RF has provided stronger overall classification performance than DT and DL for printability prediction, while retaining feature-importance estimates that help identify influential formulation variables.[61] DL achieved higher recall and produced finer printability boundaries in the same comparison. These results reflect two practical design objectives. RF supports reliable screening within an established formulation space, while DL retains a broader range of potentially printable candidates during exploratory design. Both strategies can reduce experimental effort by prioritizing formulations for targeted validation and limiting the number of low-probability candidates that proceed to material preparation and printing.

A similar balance appears in pre-printing regression. SVR has outperformed linear and regularized regression models across most evaluated bioink features, indicating that nonlinear kernels can capture relationships that are difficult to represent using fixed linear coefficients.[65] Linear and regularized models retain an advantage when transparent relationships between material descriptors and predicted outcomes are needed. The choice therefore depends on whether the immediate objective is accurate property prediction, interpretable material screening, or rapid identification of promising formulations. In each case, the practical value comes from narrowing the experimental design space before fabrication. This benefit remains dependent on material-specific validation because predictive relationships learned from one bioink family may not transfer to formulations with different chemistries, crosslinking mechanisms, or rheological behavior.

As the workflow moves into printing, the learning problem shifts from material selection to process stability and fabrication quality. Structured combinations of pressure, speed, temperature, geometry, and material properties can be modeled effectively using gradient-boosted trees. Their sequential learning structure resolves nonlinear interactions among process variables and has produced stronger print-quality predictions than alternative regression models.[81] This capability transforms parameter selection from broad trial-and-error testing into a more focused prediction-and-validation process. Fewer parameter combinations need to be printed, and conditions associated with poor geometric fidelity can be identified before they generate failed structures, material waste, or repeated machine setup.

Image-based monitoring extends this predictive role into the printing process itself. CNNs learn spatial patterns associated with layer geometry, filament continuity, surface appearance, and dimensional defects and have achieved higher classification accuracy than conventional models based on reduced image features.[140] Increasing architectural complexity can improve defect recognition, while lightweight models offer faster inference with lower computational demand. The comparison between ConvNeXt_Base and MobileNetV2 illustrates this deployment trade-off: the larger model provides the highest accuracy, while the compact model retains comparable performance and is better suited to real-time monitoring. This transition from offline prediction to continuous observation is practically important because defects can be detected as they emerge. When monitoring is connected to machine-level control, the same information can guide adjustments in pressure, flow rate, printing speed, toolpath, or exposure conditions, reducing operator-dependent variation and improving process reproducibility. Such closed-loop implementation still requires reliable sensing, low-latency inference, uncertainty-aware decisions, and validation across printers, materials, and operating environments.

After printing, the learning objective changes from controlling fabrication to extracting reliable information from the wearable device. Feature-based models remain effective when compact descriptors represent the relevant signal patterns. SVM has achieved high motion-recognition accuracy using statistical features extracted from resistance signals, while RF has outperformed gradient boosting for tactile object recognition using structured multisensor inputs.[27,145] Their moderate computational requirements

Table 8. Summary comparison of AI algorithm performance across the three-stage workflow

Stage	Task	Best-performing model	Performance	Rationale	Year & Ref.
Pre-printing	Printability classification	RF	Acc. 88.1%; F1 87.0%	Best overall performance	2023,[61]
	Candidate screening	DL	Rec. 87.3%	Higher sensitivity	2023,[61]
	Bioink prediction	SVR	Best for 83% of features	Suitable for small datasets	2026,[65]
In-process	Print-quality prediction	Gradient boosting	$R^2 = 0.954$	Captures nonlinear interactions	2022,[81]
	Real-time monitoring	ConvNeXt_Base	Acc. 0.96	Highest classification accuracy	2022,[140]
Post-printing	Motion recognition	SVM	Acc. 95.83%	Effective with limited data	2023,[145]
	Object recognition	RF	Acc. 98.32%	Stable multisensor classification	2025,[27]

Abbreviations: DL: Deep learning; RF: Random forest; SVM: Support vector machine; SVR: Support vector regression.

support rapid inference and potential integration with wearable or edge hardware. RANSAC regression provides an additional practical advantage for quantitative colorimetric sensing because it limits the influence of outlying measurements caused by imaging variation or heterogeneous sensor responses.[144] In these applications, AI increases the functional value of the printed device by converting complex electrical, mechanical, or optical responses into physiological, biochemical, or behavioral information.

Raw time-series and multimodal signals require greater representational capacity. CNNs can extract local waveform or image features, RNNs can model temporal dependencies, and hybrid architectures can integrate spatial and sequential information. These models reduce dependence on manually designed features and support more complex tasks such as gait analysis, gesture interpretation, and multimodal health assessment. Their practical performance depends on whether the learned representations remain stable across users, wearing positions, devices, and recording sessions. High accuracy within a controlled dataset does not establish reliable operation under motion, sensor drift, environmental variation, or long-term use. Cross-user testing, independent-device evaluation, and longitudinal validation therefore become increasingly important as post-printing models move from proof-of-concept classification toward continuous wearable monitoring.

Across the three stages, model complexity increases as the data progress from structured formulation descriptors to process images and multimodal wearable signals. Interpretability changes along the same path. Linear models and shallow trees provide direct relationships between inputs and predictions. RF and gradient boosting capture more complex interactions while retaining partial interpretation through feature-importance and attribution methods. Kernel models offer strong performance in small nonlinear datasets, although individual predictions are less transparent. DL models provide greater flexibility for images and sequences, while their internal representations are more difficult to connect with material, process, or physiological mechanisms.[153] Physics-informed constraints, uncertainty estimation, and interpretable feature analysis can help preserve confidence as AI assumes a more active role in manufacturing control and health-related interpretation.

The maturity of these approaches also follows the progression of the workflow. Shallow ML models for offline formulation screening, parameter prediction, and feature-based signal classification are relatively established at the laboratory scale. CNN-based inspection and lightweight edge inference are developing toward real-time implementation. Transferable closed-loop control, adaptive sensor calibration, and autonomous integration across design, fabrication, and wearable operation remain emerging capabilities. Progress toward practical implementation will therefore depend on more than increases in model accuracy. It will require standardized data acquisition, external validation, efficient inference, machine-level integration, and evidence that performance remains stable across materials, printers, devices, and users.

The available evidence supports an algorithm-selection strategy guided by both task structure and operational purpose. RF, gradient boosting, SVM, and SVR are effective for structured datasets with limited samples and can reduce experimental screening and parameter trials. CNNs are better suited to image-based monitoring, where they can support early defect detection and improve process robustness. Lightweight CNNs provide a practical balance between accuracy and real-time computational requirements. RNNs and hybrid architectures become valuable when wearable applications contain temporal dependencies or multiple sensing modalities. The most appropriate model is therefore the one that combines sufficient predictive performance with the interpretability, data efficiency, computational cost, validation evidence, and implementation readiness required by the target application.

4. Challenges and outlook

Although AI has shown promise in supporting individual stages of additively manufactured wearable biosensor development, most current studies remain task-specific and disconnected across the pre-printing, in-process, and post-printing stages. In most cases, AI is applied to one defined task, such as printability prediction, process-parameter selection, defect detection, device-performance estimation, or sensing-signal interpretation.[99] These studies reduce empirical trial and error and improve the efficiency of material and device development.[56] However, improving each step separately is not enough. Future work needs to connect material formulation, AM processing, device architecture, wearable operation, and biomedical interpretation within a continuous design-to-use workflow. Moving from isolated AI assistance to workflow-level integration is therefore a central challenge for AM-fabricated wearable biosensors.[7,154]

The difficulty begins with data. AM-fabricated wearable biosensors are governed by coupled relationships among material composition, rheology, curing behavior, printing parameters, structural fidelity, biofunctional activity, skin-device mechanics, and sensing environment.[56] Yet most datasets capture only one part of this chain. A model trained to predict ink printability may not include conductivity, adhesion, biochemical activity, or long-term signal stability.[124] A model trained to interpret sensing signals may not include the manufacturing history that contributes to device-to-device variability.[150] This separation limits the ability of AI to learn transferable relationships among processing, structure, function, and wearable performance. Future studies should move from isolated datasets toward structured data frameworks that record material descriptors, printing conditions, device geometry, fabrication quality, sensing response, and validation environment in a consistent manner. Without this shared data structure, model reuse, cross-laboratory comparison, and reliable generalization will remain difficult.

Physics-informed and hybrid modeling offer a promising response to this data limitation. Instead of relying exclusively on labeled examples, these models can incorporate governing equations, conservation laws, constitutive relationships, and boundary conditions as soft constraints during training.[155] For extrusion-based AM, mass and momentum conservation, non-Newtonian rheology, pressure-flow relationships, and curing or crosslinking kinetics could constrain predictions of filament formation, dimensional fidelity, and process stability.[156] Hybrid frameworks could further combine computational fluid dynamics (CFD) or finite element modeling (FEM) simulations with ML-based surrogate or residual models, using established process physics to describe dominant behavior and experimental data to capture material- and machine-specific deviations. Similar principles apply to post-printing biosensing, where the Nernst equation, Butler–Volmer kinetics, and diffusion-controlled mass transport could guide signal interpretation, calibration, and estimation of electrochemical parameters from limited measurements.[157] By restricting predictions to physically plausible regimes, these approaches may improve data efficiency, reduce overfitting, and connect model outputs with interpretable material, process, and sensing parameters. Their reliability will depend on the validity of the embedded physics, boundary conditions, and loss weighting. Future studies should therefore compare physics-informed, hybrid, and purely data-driven models under consistent data-scarcity conditions and evaluate their transferability across materials, printers, devices, and users.

Material design is one area where workflow integration is especially needed. Current AI studies often focus on printability, filament stability, droplet formation, curing fidelity, or shape retention. These outputs are necessary, but they do not fully define a wearable biosensor material. A printable material must also provide mechanical compliance, electrical or optical transduction, biochemical selectivity, interfacial adhesion, biocompatibility, and stability under deformation, hydration, sweat exposure, and repeated use.[1,18] Future AI-assisted material design should therefore treat wearable biosensor materials as multifunctional systems, rather than printable formulations alone. Instead of optimizing one target at a time, future models should jointly consider printability, softness, conductivity, bioactivity, durability, and sensing

stability. This is especially important for conductive hydrogels, elastomers, ionogels, biofunctional inks, and composite interfaces, where small formulation changes can simultaneously alter flow behavior, charge transport, mechanical fatigue, and sensing response.[7]

Generative design can expand the design space of AM-fabricated wearable biosensors, but the generated candidates still require careful validation.[130,131] A generated structure, morphology, material layout, or process window may appear reasonable but fail in printability, mechanical stability, biocompatibility, sensing performance, or long-term wearable reliability. Generative design should therefore be combined with printability prediction, physics-based simulation, experimental feedback, and wearable validation. Current applications are also concentrated mainly in pre-printing design. Its potential roles in in-process monitoring, closed-loop process correction, post-printing device evaluation, and real-time wearable sensing remain less explored. Future work should improve the validation of generated designs and examine how generative models can support fabrication control and post-printing performance assessment.

A systems view is also needed for AM routes. AI has been adopted more often in extrusion-based printing and photopolymerization-based printing because their process variables are easier to define and their quality metrics can often be extracted from images, geometries, or printed features.[38,56,60,81] Other routes, including screen printing, embedded printing, and 2PP, remain less represented in AI-assisted wearable biosensor fabrication.[16,110,111,113,115] This gap reflects the difficulty of measuring and modeling different process-structure-function relationships. Screen printing is important for scalable electrochemical sensing, but electrode quality depends on ink-substrate interaction, drying behavior, layer uniformity, and batch reproducibility. Embedded printing can create soft channels, suspended structures, and complex hydrogel architectures, but its outcome depends on coupled ink rheology, support-bath behavior, nozzle motion, and crosslinking dynamics. 2PP can produce high-resolution microstructured interfaces, microneedles, microfluidic features, and microscale sensing architectures, but its integration with AI is limited by small photocurable material libraries, narrow exposure windows, low-throughput data generation, and the cost of producing labeled micro- and nanoscale datasets. Future work should extend AI-guided optimization beyond the most accessible printing platforms and develop models that account for the specific physics, measurement limits, and functional outputs of underexplored AM methods.

Process intelligence is also shifting from open-loop prediction to closed-loop intervention. Several recent studies have demonstrated printing systems that combine real-time imaging, computer vision, and feedback control to regulate filament deposition, correct extrusion errors, or adapt toolpaths on moving and deformable surfaces.[14,66-68,118] These studies show that AI can participate directly in fabrication, rather than only evaluate printed outcomes after deposition. However, most current closed-loop systems remain task specific. They are usually developed for defined materials, geometries, sensing modalities, or correction targets, and their transferability to soft, biofunctional, and multimaterial wearable biosensor platforms remains limited. This limitation is important because wearable biosensor materials can change during extrusion, curing, drying, swelling, crosslinking, or contact with substrates.[18,19] These changes may affect line width, layer adhesion, electrode continuity, microfluidic geometry, and biological activity. Future closed-loop systems should therefore move beyond single-error correction and integrate real-time sensing, rapid data processing, uncertainty-aware decision-making, and direct machine-level control. For AM-fabricated wearable biosensors, this capability would allow adaptive adjustment of pressure, flow rate, printing speed, toolpath, exposure dose, layer height, or curing condition during fabrication. The next challenge is to make closed-loop control transferable across the diverse materials, structures, and sensing functions required for wearable biosensors.

Digital twins provide a possible framework for moving from isolated AI models to workflow-level integration.[158,159] For AM-fabricated wearable biosensors, a useful digital twin should not only reproduce printer motion or final device geometry. It should connect formulation design, process physics, structural evolution, device performance, body-interface mechanics, and sensing signal drift.[160] Current AI models usually address only one part of this sequence, which limits their ability to predict how a change in material composition affects printing quality, structural fidelity, mechanical response, analyte transport, and long-term sensing reliability.[7,161] Future digital twins should combine physics-based modeling, *in situ* process monitoring, experimental datasets, and AI-based prediction to represent both fabrication and wearable operation.[162] This integrated model could support material selection, process correction, personalized device design, and long-term performance prediction.

As AI-enabled wearable biosensors move toward biomedical applications, their reliability must be evaluated across fabrication batches, devices, users, and operating conditions. Variations in printed geometry, material composition, skin contact, wearing position, and environmental conditions can change baseline

responses and sensing sensitivity, limiting the transfer of a calibration model from one device or user to another. Future studies should therefore report cross-device and cross-user validation and determine when device-specific or user-specific recalibration is required. Motion-artifact reduction should also be evaluated separately from motion recognition.[163] Models intended for physiological or biochemical monitoring should be tested during body movement, changes in skin contact, and mechanical deformation to determine whether the target signal can be recovered from motion-induced interference. Long-term studies are equally important because repeated loading, sweat exposure, temperature changes, material aging, and sensor drift can alter signal quality during extended use.[164] Model evaluation should therefore include calibration stability, drift compensation, uncertainty estimation, failure-mode analysis, and longitudinal validation under realistic wearing conditions.[153]

Deployment remains a major step for AI-assisted AM-fabricated wearable biosensors. Many AI models for printed wearable biosensors are still trained and evaluated offline, whereas practical wearable systems require fast, low-power, stable, and privacy-aware inference.[56] Cloud-based analysis can support complex computation, but it may introduce latency, connectivity dependence, and data security concerns.[165] Edge intelligence should therefore be considered during device design, rather than added after fabrication. In practical wearable platforms, the sensing modality, sampling rate, power system, communication module, and model architecture are closely coupled.[166] Future systems should combine lightweight models, model compression, embedded inference, cloud-edge collaboration, and privacy-preserving learning. This direction is important for continuous health monitoring, wound management, rehabilitation, sports assessment, and point-of-care biochemical sensing.[44,167]

Based on the challenges discussed above, future research can be organized into near-, medium-, and long-term priorities. In the near term, the field needs standardized datasets that connect material composition, rheology, printing conditions, device geometry, fabrication quality, and sensing performance. Common metadata, reporting formats, benchmark tasks, and validation protocols would make results easier to compare across laboratories.[168] Transfer learning may help adapt existing models to new materials, printers, devices, or users when only limited data are available.[169] Its effectiveness, however, should be tested carefully because differences between the source and target domains may reduce performance or lead to negative transfer.

The next step is to connect standardized data with digital twins and closed-loop intelligent manufacturing. Digital twins can combine process physics, *in situ* measurements, and AI predictions to track changes in materials, printed structures, and device performance. Closed-loop systems can then use this information to adjust printing parameters when unstable deposition or defects are detected. Practical implementation will require reliable process sensing, low-latency inference, uncertainty-aware decisions, and direct communication between AI models and machine controllers. These systems must also be validated across different materials, printers, geometries, and operating conditions.

In the longer term, foundation models may provide reusable representations across material design, manufacturing data, images, sensor signals, and biomedical applications.[170,171] Such models could be adapted to specific tasks through fine-tuning or transfer learning, reducing the amount of labeled data required for each new system. Their development will depend on sufficiently large and well-curated multimodal datasets, consistent data descriptions, and access to suitable computational resources. Model bias, interpretability, privacy, and generalization across laboratories and users must also be addressed before these models can support practical or clinical decisions. Together, these steps provide a path from shared data and transferable models to digital twins, closed-loop manufacturing, and integrated AI support throughout the development and use of additively manufactured wearable biosensors.

5. Conclusion

Additively manufactured wearable biosensors combine the structural freedom of AM with the continuous monitoring capability of wearable sensing. AM enables customized geometries, soft body-conformal interfaces, spatial material patterning, and integrated sensing structures. AI adds data-driven tools for material screening, process optimization, defect recognition, device-performance prediction, and signal interpretation. In this context, AI-assisted AM can support wearable biosensors that are printable, functional, adaptive, and better matched to user-specific conditions.

This review summarized recent progress across the development chain of AI-assisted AM-fabricated wearable biosensors. At the pre-printing stage, AI has been used to predict printability, screen formulations, optimize rheological properties, select processing windows, and improve light-based printing fidelity. Generative design adds candidate generation to pre-printing design by proposing device layouts, printed morphologies, material distributions, and process windows for later screening

and validation. During fabrication, AI supports defect detection, process monitoring, parameter optimization, and emerging closed-loop correction. After printing and deployment, AI expands the function of wearable biosensors by converting complex electrical, electrochemical, optical, colorimetric, piezoresistive, triboelectric, and multimodal signals into physiological, biochemical, behavioral, tactile, and communication-level information. Despite this progress, the field remains at an early stage. Many models are trained on small or platform-specific datasets, and many demonstrations remain offline, open-loop, or limited to short-term validation. Future development should focus on integrated AI-AM-wearable systems that connect material design, fabrication quality, device performance, and real-world sensing reliability. With better datasets, interpretable models, closed-loop manufacturing, digital twins, and edge deployment, AI-assisted AM-fabricated wearable biosensors may become more reliable platforms for personalized health monitoring and biomedical use.

Acknowledgments

None.

Funding

The work was supported by the National Natural Science Foundation of China under grant no. 52201272.

Conflict of interest

Prof. Chee Kai Chua and Dr. Jia An serve as the Editor-in-Chief and the Assistant Editor of this journal, respectively, but they were not in any way involved in the editorial and peer-review process conducted for this paper, directly or indirectly. The authors declare they have no competing interests.

Author contributions

Conceptualization: Zhuoyuan Yang, Meng Cheng, Sirish Namilae, Chee Kai Chua, Yizhou Jiang

Project administration: Jia An, Meng Cheng, Chee Kai Chua, Yizhou Jiang

Supervision: Meng Cheng, Sirish Namilae, Chee Kai Chua, Yizhou Jiang

Visualization: Zhuoyuan Yang, Zefu Ren, Yuxuan Wu

Writing–original draft: Zhuoyuan Yang, Zefu Ren, Yuxuan Wu

Writing–review & editing: All authors

Ethics approval and consent to participate

Not applicable.

Consent for publication

Not applicable.

Availability of data

Not applicable.

References

1. Kim J, Campbell AS, de Ávila BE-F, Wang J. Wearable biosensors for healthcare monitoring. *Nat Biotechnol*. 2019;37(4):389-406.

   doi: 10.1038/s41587-019-0045-y

2. Iqbal SMA, Mahgoub I, Du E, Leavitt MA, Asghar W. Advances in healthcare wearable devices. *npj Flexible Electron*. 2021;5(1):9.

   doi: 10.1038/s41528-021-00107-x

3. Wicaksono I, Tucker CI, Sun T, *et al*. A tailored, electronic textile conformable suit for large-scale spatiotemporal physiological sensing in vivo. *npj Flexible Electron*. 2020;4(1):5.

   doi: 10.1038/s41528-020-0068-y

4. Liu Y, Pharr M, Salvatore GA. Lab-on-Skin: A Review of Flexible and Stretchable Electronics for Wearable Health Monitoring. *ACS Nano*. 2017;11(10):9614-9635.

   doi: 10.1021/acsnano.7b04898

5. Duan H, Peng S, He S, *et al*. Wearable electrochemical biosensors for advanced healthcare monitoring. *Adv Sci*. 2025;12(2):2411433.

   doi: 10.1002/advs.202411433

6. Suryaprabha T, Choi C, Wu Y, Liu L, Hwang B. Smart wearable and implantable biosensors for continuous health monitoring: materials, biocompatibility, and AI integration. *npj Flexible Electron*. 2026;10(1):46.

   doi: 10.1038/s41528-026-00560-6

7. Ates HC, Nguyen PQ, Gonzalez-Macia L, *et al*. End-to-end design of wearable sensors. *Nat Rev Mater*. 2022;7(11):887-907.

   doi: 10.1038/s41578-022-00460-x

8. Mahato K, Saha T, Ding S, Sandhu SS, Chang A-Y, Wang J. Hybrid multimodal wearable sensors for comprehensive health monitoring. *Nat Electron*. 2024;7(9):735-750.

   doi: 10.1038/s41928-024-01247-4

9. Fan W, He Q, Meng K, *et al*. Machine-knitted washable sensor array textile for precise epidermal physiological signal monitoring. *Sci Adv*. 2020;6(11):eaay2840.

   doi: 10.1126/sciadv.aay2840

10. Qaiser N, Suryaprabha T, Vetrano F, Hwang B, Elatab N. Mechanics and bio-interface engineering in flexible biosensors for continuous health monitoring. *npj Flexible Electron*. 2026;10(1):23.

    doi: 10.1038/s41528-025-00524-2

11. Vaghasiya JV, Mayorga-Martinez CC, Pumera M. Wearable sensors for telehealth based on emerging materials and nanoarchitectonics. *npj Flexible Electron*. 2023;7(1):26.

    doi: 10.1038/s41528-023-00261-4

12. Qiu Y, Zou Z, Zou Z, *et al*. Deep-learning-assisted printed liquid metal sensory system for wearable applications and boxing training. *npj Flexible Electron*. 2023;7(1):37.

    doi: 10.1038/s41528-023-00272-1

13. Wang P, Wang G, Sun G, *et al*. A flexible-integrated multimodal hydrogel-based sensing patch. *Nano Micro Lett*. 2025;17(1):156.

    doi: 10.1007/s40820-025-01656-w

14. Kelly D, Sergis V, Ventura i Blanco L, Mason K, Daly AC. Autonomous control of extrusion bioprinting using convolutional neural networks. *Adv Funct Mater*. 2025;35(30):2424553.

    doi: 10.1002/adfm.202424553

15. Lu W-x, Fang P, Zhu M-l, *et al*. Artificial intelligence–enabled gesture-language-recognition feedback system using strain-sensor-arrays-based smart glove. *Adv Intell Syst*. 2023;5(8):2200453.

    doi: 10.1002/aisy.202200453

16. Chen B, Dong J, Ruelas M, *et al*. Artificial Intelligence-assisted high-throughput screening of printing conditions of hydrogel architectures for accelerated diabetic wound healing. *Adv Funct Mater*. 2022;32(38):2201843.

    doi: 10.1002/adfm.202201843

17. Song Y, Tay RY, Li J, *et al*. 3D-printed epifluidic electronic skin for machine learning–powered multimodal health surveillance. *Sci Adv*. 2023;9(37):eadi6492.

    doi: 10.1126/sciadv.adi6492

18. Ng WL, An J, Chua CK. Process, material, and regulatory considerations for 3D printed medical devices and tissue constructs. *Engineering*. 2024;36:146-166.

    doi: 10.1016/j.eng.2024.01.028

19. Chua CK, An J, Fan S, *et al*. A perspective on transformative bioprinting. *Int J Bioprint*. 2024;11(1):1-29.

    doi: 10.36922/ijb.3525

20. Su J, Ng WL, An J, Yeong WY, Chua CK, Sing SL. Achieving sustainability by additive manufacturing: a state-of-the-art review and perspectives. *Virtual Phys Prototyping*. 2024;19(1):e2438899.

    doi: 10.1080/17452759.2024.2438899

21. Etefagh AH, Razfar MR. Bayesian optimization of 3D bioprinted polycaprolactone/magnesium oxide nanocomposite scaffold using a machine learning technique. *Proc Inst Mech Eng, Part B: J Eng Manuf*. 2024;238(10):1448-1462.

    doi: 10.1177/09544054231202219

22. Mohammadrezaei D, Podina L, Silva JD, Kohandel M. Cell viability prediction and optimization in extrusion-based bioprinting via neural network-based Bayesian optimization models. *Biofabrication*. 2024;16(2):025016.

    doi: 10.1088/1758-5090/ad17cf

23. Qiao Q, Zhang X, Yan Z, *et al*. The use of machine learning to predict the effects of cryoprotective agents on the GelMA-based bioinks used in extrusion cryobioprinting. *Bio-Des Manuf*. 2023;6(4):464-477.

    doi: 10.1007/s42242-023-00244-4

24. Shi J, Song J, Song B, Lu WF. Multi-Objective Optimization Design through Machine Learning for Drop-on-Demand Bioprinting. *Engineering*. 2019;5(3):586-593.

    doi: 10.1016/j.eng.2018.12.009

25. Shetty A, Fathima A, Anika B, *et al*. Computational optimization of 3D printed bone scaffolds using orthogonal array-driven FEA and neural network modeling. *Sci Rep*. 2025;15(1):30515.

    doi: 10.1038/s41598-025-15122-5

26. Zhuo F, Zhou J, Liu Y, *et al*. Kirigami-Inspired 3D-Printable MXene Organohydrogels for Soft Electronics. *Adv Funct Mater*. 2023;33(52):2308487.

    doi: 10.1002/adfm.202308487

27. Pak K, Yang JC, Sim JY, *et al*. Fabrication of multifunctional wearable interconnect E-textile platform using direct ink writing (DIW) 3D printing. *npj Flexible Electron*. 2025;9(1):48.

    doi: 10.1038/s41528-025-00414-7

28. Bonatti AF, Vozzi G, Chua CK, Maria C. A Deep Learning Quality Control Loop of the Extrusion-based Bioprinting Process. *Int J Bioprint*. 2022;8(4):620.

    doi: 10.18063/ijb.v8i4.620

29. Tan HW, Tran T, Chua CK. A review of printed passive electronic components through fully additive manufacturing methods. *Virtual Phys Prototyping*. 2016;11(4):271-288.

    doi: 10.1080/17452759.2016.1217586

30. Gao H, An J, Chua CK, Bourell D, Kuo C-N, Tan DTH. 3D printed optics and photonics: Processes, materials and applications. *Mater Today*. 2023;69:107-132.

    doi: 10.1016/j.mattod.2023.06.019

31. Shinde S, Kim KH, Pawar O, Patil OA, Lim S, Lee HE. 3D-printable alginate-MoS2-AgNW hydrogel bioink for dual-mode wearable capacitive biosensors. *Int J Bioprint*. 2025;11(5):301.

    doi: 10.36922/ijb025290295

32. Tang K, Yang Z, Cheng M, *et al*. 3D-printed multi-stage helical continuous carbon fiber based supercapacitors

with enhanced mechanical performance. *J Energy Storage*. 2026;148:120354.

doi: 10.1016/j.est.2026.120354

33. Levato R, Dudaryeva O, Garciamendez-Mijares CE, *et al*. Light-based vat-polymerization bioprinting. *Nat Rev Methods Primers*. 2023;3(1):47.

doi: 10.1038/s43586-023-00231-0

34. Poltue T, Montgomery SM, Sun X, *et al*. Machine learning-based optimization of pixel light intensities for improving polymerization accuracy in digital light processing 3D printing. *Adv Mater Technol*. 2025;10(20):e00902.

doi: 10.1002/admt.202500902

35. Ma Y, Tian Z, Wang B, *et al*. Enhancing the 3D printing fidelity of vat photopolymerization with machine learning-driven boundary prediction. *Mater Des*. 2024;241:112978.

doi: 10.1016/j.matdes.2024.112978

36. Guan J, You S, Xiang Y, *et al*. Compensating the cell-induced light scattering effect in light-based bioprinting using deep learning. *Biofabrication*. 2021;14(1):015011

doi: 10.1088/1758-5090/ac3b92

37. Xu H, Liu Q, Casillas J, *et al*. Prediction of cell viability in dynamic optical projection stereolithography-based bioprinting using machine learning. *J Intell Manuf*. 2022;33(4):995-1005.

doi: 10.1007/s10845-020-01708-5

38. Nam J, Chen B, Kim M. Machine learning-driven grayscale digital light processing for mechanically robust 3D-printed gradient materials. *Adv Mater*. 2025;37(42):2504075.

doi: 10.1002/adma.202504075

39. Maleki H, Asadi P, Akbari M, Peyghami M, Salarvand V, Bedir F. Incorporation of machine learning in the design of bio-nanocomposites produced by DLP 3D printer. *Results Eng*. 2025;27:105756.

doi: 10.1016/j.rineng.2025.105756

40. Chen X, Chen C, Zeng H, *et al*. 3D-printed microstructured ionic hydrogel and nano-friction generator for self-powered electronic skin and deep learning character recognition. *Chem Eng J*. 2026;530:173579.

doi: 10.1016/j.cej.2026.173579

41. Lin SS-r, Gamage NM, Herath K, Withana A. MyoSpring: 3D Printing Mechanomyographic Sensors for Subtle Finger Gesture Recognition. In: Proceedings of the Sixteenth International Conference on Tangible, Embedded, and Embodied Interaction. February 13-16, 2022; Daejeon, Korea. ACM. 2022:1-13.

doi: 10.1145/3490149.3501321

42. Xie Y, Li K, Liu J, *et al.* A smart lab on a wearable microneedle patch with convolutional neural network-enhanced colorimetry for early warning of syndrome of inappropriate antidiuretic hormone secretion. *Aggregate*. 2025;6(2):e671.

doi: 10.1002/agt2.671

43. Wang X, Liu J, Dong R, Gilchrist MD, Zhang N. High-precision digital light processing (DLP) printing of microstructures for microfluidics applications based on a machine learning approach. *Virtual Phys Prototyping*. 2024;19(1):e2318774.

doi: 10.1080/17452759.2024.2318774

44. Saadi OW, Khan KA. Advancements in vat photopolymerization for piezoresistive sensors: materials, mechanisms, and applications. *Virtual Phys Prototyping*. 2025;20(1):e2505994.

doi: 10.1080/17452759.2025.2505994

45. Ren Z, Yang Z, Srinivasaraghavan Govindarajan R, *et al*. Two-Photon Polymerization of Bioinspired Microstructure with Tunable Wettability Controlled by Dielectric Elastomer Actuator. *ACS Appl Mater Interfaces*. 2025;17(45):62662-62671.

doi: 10.1021/acsami.5c10911

46. Sun J, Yao K, An J, Jing L, Huang K, Huang D. Machine learning and 3D bioprinting. *Int J Bioprint*. 2023;9(4):717.

doi: 10.18063/ijb.717

47. Wang X, Dong W, Dong H, *et al*. Bioprinting of wearable sensors, brain-machine interfaces, and exoskeleton robots. *Int J Bioprint*. 2024;10(6):3590.

doi: 10.36922/ijb.3590

48. Gharraei R, Bergstrom DJ, Chen X. Extrusion bioprinting from a fluid mechanics perspective. *Int J Bioprint*. 2024;10(6):3973.

doi: 10.36922/ijb.3973

49. Seneviratne S, Hu Y, Nguyen T, *et al*. A Survey of Wearable Devices and Challenges. *IEEE Communications Surveys & Tutorials*. 2017;19(4):2573-2620.

doi: 10.1109/COMST.2017.2731979

50. Wang AYL, Aviña AE, Liu Y-Y, Kao H-K. Skin bioprinting for burn reconstruction: From stem cell integration to smart in situ regenerative systems. *Int J Bioprint*. 2025;11(6):130.

doi: 10.36922/ijb025360364

51. Roy A, Zenker S, Jain S, *et al*. A highly stretchable, conductive, and transparent bioadhesive hydrogel as a flexible sensor for enhanced real-time human health monitoring. *Adv Mater*. 2024;36(35):2404225.

doi: 10.1002/adma.202404225

52. Wang Y, Bai H, Ren Y, Yang Y, Wang J. Artificial intelligence-augmented bioprinting systems: Data-driven optimization and future applications in pharmacological research. *Int J Bioprint*. 2025;11(6):025350349.

doi: 10.36922/ijb025350349

53. Quan R, Liu F, Chinchilla SC. Integrating machine learning and finite element simulation for interpretable prediction of 3D-printed bone scaffold mechanics. *Int J Bioprint*. 2025;11(6):025270257.

doi: 10.36922/ijb025270257

54. Garg A, Sharma A, Zheng W, Li L. A review on artificial intelligence-enabled mechanical analysis of 3D printed and FEM-modelled auxetic metamaterials. *Virtual Phys Prototyping*. 2025;20(1):e2445712.

doi: 10.1080/17452759.2024.2445712

55. Yin X, Akmal J, Salmi M. Artificial intelligence-driven defect detection and localization in metal 3D printing using convolutional neural networks. *Mater Sci Addit Manuf*. 2025;4(3):025150022.

doi: 10.36922/msam025150022

56. Cui F, Yue Y, Zhang Y, Zhang Z, Zhou HS. Advancing Biosensors with Machine Learning. *ACS Sens*. 2020;5(11):3346-3364.

doi: 10.1021/acssensors.0c01424

57. Bhaiyya M, Panigrahi D, Rewatkar P, Haick H. Role of machine learning assisted biosensors in point-of-care-testing for clinical decisions. *ACS Sens*. 2024;9(9):4495-4519.

doi: 10.1021/acssensors.4c01582

58. Sidey-Gibbons JAM, Sidey-Gibbons CJ. Machine learning in medicine: a practical introduction. *BMC Med Res Methodol*. 2019;19(1):64.

doi: 10.1186/s12874-019-0681-4

59. LeCun Y, Bengio Y, Hinton G. Deep learning. *Nature*. 2015;521(7553):436-444.

doi: 10.1038/nature14539

60. Lee J, Oh SJ, An SH, Kim W-D, Kim S-H. Machine learning-based design strategy for 3D printable bioink: elastic modulus and yield stress determine printability. *Biofabrication*. 2020;12(3):035018.

doi: 10.1088/1758-5090/ab8707

61. Chen H, Liu Y, Balabani S, Hirayama R, Huang J. Machine learning in predicting printable biomaterial formulations for direct ink writing. *Research*. 2023;6:0197.

doi: 10.34133/research.0197

62. Kim T, Kim D, Kwon S-S, Sing SL, Kim N, Jung ID. Reinforcement learning-based toolpath optimisation with 3D U-Net driven rapid thermal prediction. *Virtual Phys Prototyping*. 2026;21(1):e2627765.

doi: 10.1080/17452759.2026.2627765

63. Chen Y, Han P, Vandi L-J, *et al*. A biocompatible thermoset polymer binder for Direct Ink Writing of porous titanium scaffolds for bone tissue engineering. *Mater Sci Eng C*. 2019;95:160-165.

doi: 10.1016/j.msec.2018.10.033

64. Hashemi A, Ezati M, Zumberg I, *et al*. Characterization and optimization of a biomaterial ink aided by machine learning-assisted parameter suggestion. *Mater Today Commun*. 2024;40:109777.

doi: 10.1016/j.mtcomm.2024.109777

65. da Silva VA, Yu B, Willerth SM. Early-stage material properties as predictors of neural bioink performance during extrusion 3D bioprinting. *Biofabrication*. 2026;18(2):025002.

doi: 10.1088/1758-5090/ae46e2

66. Zhu Z, Guo S-Z, Hirdler T, *et al*. 3D Printed Functional and Biological Materials on Moving Freeform Surfaces. *Adv Mater*. 2018;30(23):1707495.

doi: 10.1002/adma.201707495

67. Zhu Z, Park HS, McAlpine MC. 3D printed deformable sensors. *Sci Adv*. 2020;6(25):eaba5575.

doi: 10.1126/sciadv.aba5575

68. Jeong S-H, Kim J, Thibault BC, *et al*. Intelligent In situ Printing of Multimaterial Bioinks for First-Aid Wound Care Guided by Eye-In-Hand Robot Technology. *Adv Mater Technol*. 2024;9(11):2400060.

doi: 10.1002/admt.202400060

69. Kumar D, Liu Y, Song H, Namilae S. Explainable deep neural network for in-plain defect detection during additive manufacturing. *Rapid Prototyping J*. 2023;30(1):49-59.

doi: 10.1108/rpj-05-2023-0157

70. Kumar D, Phillips NA, Liu Y, Namilae S. Multisource data fusion for defect detection in composite additive manufacturing using explainable deep neural network. *Aerosp Sci Technol*. 2024;155:109729.

doi: 10.1016/j.ast.2024.109729

71. Fu Z, Angeline V, Sun W. Evaluation of Printing Parameters on 3D Extrusion Printing of Pluronic Hydrogels and Machine Learning Guided Parameter Recommendation. *Int J Bioprint*. 2021;7(4):434.

doi: 10.18063/ijb.v7i4.434

72. Tian S, Stevens R, McInnes BT, Lewinski NA. Machine Assisted Experimentation of Extrusion-Based Bioprinting Systems. *Micromachines*. 2021;12(7):780.

doi: 10.3390/mi12070780

73. Barši Palmić T, Podlipnik E, Slavič J. Single-process 3D-printed smart pad with CNN-based touch localization and force classification. *Virtual Phys Prototyping*. 2026;21(1):e2640277.

doi: 10.1080/17452759.2026.2640277

74. Hu B, Cheng M, Yang Z, *et al*. Multi-material 3D printing of self-powered sensors based on ionic thermoelectric hydrogels. *Virtual Phys Prototyping*. 2026;21(1):e2638660.

doi: 10.1080/17452759.2026.2638660

75. Yang Z, Medora E, Ren Z, Cheng M, Namilae S, Jiang Y. Coaxial direct ink writing of ZnO functionalized continuous carbon fiber-reinforced thermosetting composites. *Compos Sci Technol*. 2024;256:110782.

doi: 10.1016/j.compscitech.2024.110782

76. Li X, Liu S, Mo J, *et al*. A programmable bioresorbable electrochemical microneedle sensor array for perioperative monitoring of organ health. *Nat Biomed Eng*. 2026:1-18

doi: 10.1038/s41551-025-01609-z

77. Li X, Zheng S, He M, *et al*. Self-calibrating multiplexed microneedle electrode array for continuous mapping of subcutaneous multi-analytes in diabetes. *The Innovation*. 2025;6(2):100781.

doi: 10.1016/j.xinn.2024.100781

78. Jin Z, Zhang Z, Shao X, Gu GX. Monitoring anomalies in 3D bioprinting with deep neural networks. *ACS Biomater Sci Eng*. 2023;9(7):3945-3952.

doi: 10.1021/acsbiomaterials.0c01761

79. Chen Y, Non J, Vozovik Z, Kim WS. AI-enhanced diagnosis of atrial arrhythmia using 3D-printed origami ECG sensors. *Biosens Bioelectron*. 2026;292:118069.

doi: 10.1016/j.bios.2025.118069

80. Bocan A, Siavash Moakhar R, del Real Mata C, *et al*. Machine-learning-aided advanced electrochemical biosensors. *Adv Mater*. 2025;37(33):2417520.

doi: 10.1002/adma.202417520

81. Rahmani Dabbagh S, Ozcan O, Tasoglu S. Machine learning-enabled optimization of extrusion-based 3D printing. *Methods*. 2022;206:27-40.

doi: 10.1016/j.ymeth.2022.08.002

82. Nadernezhad A, Groll J. Machine learning reveals a general understanding of printability in formulations based on rheology additives. *Adv Sci*. 2022;9(29):2202638.

doi: 10.1002/advs.202202638

83. Yi H, Guo X, Chang F, Cao H, An J, Chua CK. Ink-jetting-based conformal additive manufacturing: advantages, opportunities, and challenges. *Int J Extreme Manuf*. 2025;7(3):032002.

doi: 10.1088/2631-7990/ada8e6

84. Giordano GF, Ferreira LF, Bezerra ÍRS, *et al*. Machine learning toward high-performance electrochemical sensors. *Anal Bioanal Chem*. 2023;415(18):3683-3692.

doi: 10.1007/s00216-023-04514-z

85. Hinton GE, Salakhutdinov RR. Reducing the Dimensionality of Data with Neural Networks. *Science*. 2006;313(5786):504-507.

doi: 10.1126/science.1127647

86. Yu K, Yao Y, Zhang W, *et al*. Defects, monitoring, and AI-enabled control in soft material additive manufacturing: a review. *Virtual Phys Prototyping*. 2025;20(1):e2588456.

doi: 10.1080/17452759.2025.2588456

87. Guerrero F, Ortiz AR, Thomson P, Gomez D. Hierarchical bayesian model selection for three-dimensional-printed cementitious materials. *Mater Sci Addit Manuf*. 2026;5(2):025460109.

doi: 10.36922/msam025460109

88. Breiman L. Random Forests. *Mach Learn*. 2001;45(1):5-32.

doi: 10.1023/A:1010933404324

89. Cortes C, Vapnik V. Support-vector networks. *Mach Learn*. 1995;20(3):273-297.

doi: 10.1007/BF00994018

90. Quinlan JR. Induction of decision trees. *Mach Learn*. 1986;1(1):81-106.

doi: 10.1007/BF00116251

91. Friedman JH. Greedy function approximation: A gradient boosting machine. *Ann Stat*. 2001;29(5):1189-1232,44.

doi: 10.1214/aos/1013203451

92. Cover T, Hart P. Nearest neighbor pattern classification. *IEEE Trans Inf Theor*. 1967;13(1):21-27.

doi: 10.1109/tit.1967.1053964

93. Rumelhart DE, Hinton GE, Williams RJ. Learning representations by back-propagating errors. *Nature*. 1986;323(6088):533-536.

doi: 10.1038/323533a0

94. Lecun Y, Bottou L, Bengio Y, Haffner P. Gradient-based learning applied to document recognition. *Proc IEEE*. 1998;86(11):2278-2324.

doi: 10.1109/5.726791

95. Vaswani A, Shazeer N, Parmar N, *et al*. Attention is all you need. Presented at: Proceedings of the 31st International Conference on Neural Information Processing Systems. Long Beach, CA; 2017.

doi: 10.48550/arXiv.1706.03762

96. Pearson K. LIII. On lines and planes of closest fit to systems of points in space. *London Edinburgh Philos Mag & J Sci*. 1901;2(11):559-572.

doi: 10.1080/14786440109462720

97. Snoek J, Larochelle H, Adams RP. Practical Bayesian optimization of machine learning algorithms. Presented at: Proceedings of the 26th International Conference on Neural

Information Processing Systems. Volume 2. Lake Tahoe, Nevada; 2012.

doi: 10.48550/arXiv.1206.2944

98. Creswell A, White T, Dumoulin V, Arulkumaran K, Sengupta B, Bharath AA. Generative Adversarial Networks: An Overview. *IEEE Signal Process Mag*. 2018;35(1):53-65.

doi: 10.1109/MSP.2017.2765202

99. Chen H, Huang J. Advancing sustainability in bioprinting through artificial intelligence. *Int J Bioprint*. 2025;11(4):025170164.

doi: 10.36922/ijb025170164

100. Qin L, Qian X, Xu D, *et al*. Personalized antimicrobial and soundproof earplugs through embedded-suspension 3D printing of polydimethylsiloxane-Ag composites for the prevention of swimmers' otitis externa. *Mater Sci Addit Manuf*. 2025;5(1):025260054.

doi: 10.36922/msam025260054

101. Mendoza-Cerezo L, Rodríguez-Rego JM, Macías-García A, Díaz-Prado SM, Marcos-Romero AC. A quantitative calibration strategy for reproducible extrusion-based bioprinting using gelatin methacryloyl hydrogels. *Int J Bioprint*. 2026;12(2):025480500.

doi: 10.36922/ijb025480500

102. Niyagama WW, Kumar SS, Puttonen T, Partanen J. Development of a compact multi-material vat photopolymerization printing solution. *Mater Sci Addit Manuf*. 2026;5(2):025510122.

doi: 10.36922/msam025510122

103. Yang Z, Tang K, Song W, *et al*. Coaxial direct writing of ultra-strong supercapacitors with braided continuous carbon fiber based electrodes. *Chem Eng J*. 2024;499:155875.

doi: 10.1016/j.cej.2024.155875

104. Wu Y, Yang Z, Madiyar F, Jiang Y, Namilae S. Hydroxyapatite functionalized natural fiber-reinforced composites: Interfacial modification and additive manufacturing. *Polym Compos*. 2025;46(1):141-155.

doi: 10.1002/pc.28974

105. Gbaguidi A, Madiyar F, Kim D, Namilae S. Multifunctional inkjet printed sensors for MMOD impact detection. *Smart Mater Struct*. 2020;29(8):085052.

doi: 10.1088/1361-665X/ab98eb

106. Dinuwan Gunawardhana KRS, Simorangkir RBVB, McGuinness GB, *et al*. The potential of electrospinning to enable the realization of energy-autonomous wearable sensing systems. *ACS Nano*. 2024;18(4):2649-2684.

doi: 10.1021/acsnano.3c09077

107. Singh SK, Rai N, Subramanian A. Machine learning-informed predictive design and analysis of electrohydrodynamic printing systems. *Adv Eng Mater*. 2023;25(19):2300740.

doi: 10.1002/adem.202300740

108. Zhang H, Yu Y, Liu X, *et al*. Autonomous printing process optimisation and in-situ anomaly detection in fused deposition modelling using an integrated data-driven approach. *Virtual Phys Prototyping*. 2025;20(1):e2545523.

doi: 10.1080/17452759.2025.2545523

109. Yu B, Zhang H, Tang J, *et al*. Multi-view deep information fusion framework for online quality monitoring and autonomous correction in material extrusion additive manufacturing. *Virtual Phys Prototyping*. 2025;20(1):e2500672.

doi: 10.1080/17452759.2025.2500672

110. Pohanka M. Screen Printed Electrodes in Biosensors and Bioassays. A Review. *Int J Electrochem Sci*. 2020;15(11):11024-11035.

doi: 10.20964/2020.11.19

111. Metters JP, Kadara RO, Banks CE. New directions in screen printed electroanalytical sensors: an overview of recent developments. *Analyst*. 2011;136(6):1067-1076.

doi: 10.1039/C0AN00894J

112. Xu Y, Mao H, Liu C, *et al*. Hopping light vat photopolymerization for multiscale fabrication. *Small*. 2023;19(11):2205784.

doi: 10.1002/smll.202205784

113. Xing J-F, Zheng M-L, Duan X-M. Two-photon polymerization microfabrication of hydrogels: an advanced 3D printing technology for tissue engineering and drug delivery. *Chem Soc Rev*. 2015;44(15):5031-5039.

doi: 10.1039/C5CS00278H

114. Song J, Michas C, Chen CS, White AE, Grinstaff MW. From Simple to Architecturally Complex Hydrogel Scaffolds for Cell and Tissue Engineering Applications: Opportunities Presented by Two-Photon Polymerization. *Adv Healthcare Mater*. 2020;9(1):1901217.

doi: 10.1002/adhm.201901217

115. Lee XY, Saha SK, Sarkar S, Giera B. Automated detection of part quality during two-photon lithography via deep learning. *Addit Manuf*. 2020;36:101444.

doi: 10.1016/j.addma.2020.101444

116. Zhang X, Li Z, Wang S, *et al*. Technological progress and challenges of volumetric additive manufacturing technology. *Virtual Phys Prototyping*. 2026:e2617762.

doi: 10.1080/17452759.2026.2617762

117. Florczak S, Größbacher G, Ribezzi D, *et al*. Adaptive and context-aware volumetric printing. *Nature*. 2025;645(8079):108-114.

doi: 10.1038/s41586-025-09436-7

118. Arduengo J, Hascoët N, Chinesta F, Hascoet J-Y. Closed-

Loop Control of Extrusion-Based Bioprinting Through Real-Time Computer Vision. *J Mach Eng*. 2025;25(2):28-42.

doi: 10.36897/jme/205422

119. Zhu Q, Van Vliet K, Holten-Andersen N, Miserez A. A Double-Layer Mechanochromic Hydrogel with Multidirectional Force Sensing and Encryption Capability. *Adv Funct Mater*. 2019;29(14):1808191.

doi: 10.1002/adfm.201808191

120. Farber E, Orlov A, Popovich A. Design and characterization of additively manufactured energy-absorbing mechanical metamaterials with bioinspired geometries. *Mater Sci Addit Manuf*. 2026;5(2):025360082.

doi: 10.36922/msam025360082

121. Asim S, Tabish TA, Liaqat U, Ozbolat IT, Rizwan M. Advances in gelatin bioinks to optimize bioprinted cell functions. *Adv Healthcare Mater*. 2023;12(17):2203148.

doi: 10.1002/adhm.202203148

122. Naghieh S, Chen X. Printability–A key issue in extrusion-based bioprinting. *J Pharm Anal*. 2021;11(5):564-579.

doi: 10.1016/j.jpha.2021.02.001

123. Lai J, Wang C, Wang M. 3D printing in biomedical engineering: Processes, materials, and applications. *Appl Phys Rev*. 2021;8(2):021322.

doi: 10.1063/5.0024177

124. Sarah R, Schimmelpfennig K, Rohauer R, Lewis CL, Limon SM, Habib A. Characterization and machine learning-driven property prediction of a novel hybrid hydrogel bioink considering extrusion-based 3D bioprinting. *Gels*. 2025;11(1):45.

doi: 10.3390/gels11010045

125. Deng B, Chen S, Lasaosa FL, *et al*. Predicting rheological properties of HAMA/GelMA hybrid hydrogels via machine learning. *J Mech Behav Biomed Mater*. 2025;168:107005.

doi: 10.1016/j.jmbbm.2025.107005

126. Rane A, Hart S, Ramesh S, Deep A. Surrogate-assisted multi-objective Bayesian optimization for improved rheological design of bioinks. *Manuf Lett*. 2024;41:1405-1414.

doi: 10.1016/j.mfglet.2024.09.167

127. Sharma M, Seiti M. Machine learning-based printability assessment and process control of aerosol jet 2D and 3D Printed PEDOT:PSS-based microstructures. *Virtual Phys Prototyping*. 2025;20(1):e2575397.

doi: 10.1080/17452759.2025.2575397

128. Toptaş M, Yılmaz M. Comparative and experimentally validated surrogate machine learning framework for predicting airflow velocity in EHD thrusters. *Int J Heat Fluid Flow*. 2026;119:110315.

doi: 10.1016/j.ijheatfluidflow.2026.110315

129. Gao W, Zhang Y, Ramanujan D, *et al*. The status, challenges, and future of additive manufacturing in engineering. *Comput-Aided Des*. 2015;69:65-89.

doi: 10.1016/j.cad.2015.04.001

130. Pugliese R, Badini S, Frontoni E, Regondi S. Generative artificial intelligence for advancing discovery and design in biomateriomics. *Intell Comput*. 2025;4:0117.

doi: 10.34133/icomputing.0117

131. Shen SC-y, Buehler MJ. Nature-inspired architected materials using unsupervised deep learning. *Commun Eng*. 2022;1(1):37.

doi: 10.1038/s44172-022-00037-0

132. Fang Z, Wang Z, Xiong J, Zhou X. Numerical characterization on mechanical performances of artificial cuttlebone-like structures produced via the generative adversarial network. *Mater Today Commun*. 2023;37:106900.

doi: 10.1016/j.mtcomm.2023.106900

133. Buehler MJ. Generating 3D architectured nature-inspired materials and granular media using diffusion models based on language cues. *Oxford Open Mater Sci*. 2022;2(1):itac010.

doi: 10.1093/oxfmat/itac010

134. Lew AJ, Buehler MJ. Single-shot forward and inverse hierarchical architected materials design for nonlinear mechanical properties using an Attention-Diffusion model. *Mater Today*. 2023;64:10-20.

doi: 10.1016/j.mattod.2023.03.007

135. Zhang C, Elvitigala KCML, Sakai S. Generative AI-guided in silico closed-loop optimisation of deposition morphology for 3D bioprinting applications. *Virtual Phys Prototyp*. 2026;21(1):e2671497.

doi: 10.1080/17452759.2026.2671497

136. Luu RK, Buehler MJ. BioinspiredLLM: Conversational large language model for the mechanics of biological and bio-inspired materials. *Adv Sci*. 2024;11(10):2306724.

doi: 10.1002/advs.202306724

137. Buehler MJ. Cephalo: Multi-modal vision-language models for bio-inspired materials analysis and design. *Adv Funct Mater*. 2024;34(49):2409531.

doi: 10.1002/adfm.202409531

138. Ghafarollahi A, Buehler MJ. SciAgents: Automating scientific discovery through bioinspired multi-agent intelligent graph reasoning. *Adv Mater*. 2025;37(22):2413523.

doi: 10.1002/adma.202413523

139. Wang L, Jiang J, Dong Y, Ghita O, Zhu Y, Sucala VI. Machine learning enabled 3D printing parameter settings for desired mechanical properties. *Virtual Phys Prototyping*. 2024;19(1):e2425825.

doi: 10.1080/17452759.2024.2425825

140. Rezapour Sarabi M, Alseed MM, Karagoz AA, Tasoglu S. Machine Learning-Enabled Prediction of 3D-Printed Microneedle Features. *Biosensors*. 2022;12(7):491.

doi: 10.3390/bios12070491

141. Ruberu K, Senadeera M, Rana S, *et al*. Coupling machine learning with 3D bioprinting to fast track optimisation of extrusion printing. *Appl Mater Today*. 2021;22:100914.

doi: 10.1016/j.apmt.2020.100914

142. Bone JM, Childs CM, Menon A, *et al*. Hierarchical Machine Learning for High-Fidelity 3D Printed Biopolymers. *ACS Biomater Sci Eng*. 2020;6(12):7021-7031.

doi: 10.1021/acsbiomaterials.0c00755

143. Bediaga-Bañeres H, Moreno-Benítez I, Arrasate S, *et al*. Artificial intelligence-driven modeling for hydrogel three-dimensional printing: computational and experimental cases of study. *Polymers*. 2025;17(1):121.

doi: 10.3390/polym17010121

144. Skonta A, Bellou MG, Stamatis H. 3D-Printed PLA hollow microneedles loaded with chitosan nanoparticles for colorimetric glucose detection in sweat using machine learning. *Biosensors*. 2025;15(7):461.

doi: 10.3390/bios15070461

145. Hou Y, Gao M, Gao J, *et al*. 3D Printed Conformal Strain and Humidity Sensors for Human Motion Prediction and Health Monitoring via Machine Learning. *Adv Sci*. 2023;10(36):2304132.

doi: 10.1002/advs.202304132

146. Young S, Zhou H, Alici G. Gesture recognition framework for teleoperation of infrared (IR) consumer devices using a novel pFMG soft armband. *Sensors*. 2024;24(18):6124.

doi: 10.3390/s24186124

147. Zhou Z, Zhang W, Zhang Y, Yin X, Chen X-Y, He B. Facile and direct 3D printing of smart glove for gesture monitoring. *Microelectron Eng*. 2023;282:112102.

doi: 10.1016/j.mee.2023.112102

148. Zhang X, Huang B, Xu K, Ge SS, Wei X. 3D printing of self-powered piezoelectric sensors enabled gait recognition via deep learning. *J Mater Chem C*. 2025;13(29):14875-14885.

doi: 10.1039/D5TC01211B

149. Truong H, Nguyen P, Nguyen A, Bui N, Vu T. Capacitive Sensing 3D-printed Wristband for Enriched Hand Gesture Recognition. In: Proceedings of the 2017 Workshop on Wearable Systems and Applications. ACM;2017:11-15.

doi: 10.1145/3089351.3089359

150. Zhang P, Guo C, Huang L, Li Y, Zhang K, Zhang Y. Highly Stretchable Serpentine-Shaped Strain Sensor Based on 3-D Printing for Gestures Recognition. *IEEE Trans Instrum Meas*. 2024;73:1-7.

doi: 10.1109/TIM.2024.3488139

151. Liu S, Hu M, Li X, *et al*. Topology-regulated 3D printed PDMS foams with conformal polydopamine/Ag interfaces for piezoresistive sensing. *Polymer*. 2026;358:130171.

doi: 10.1016/j.polymer.2026.130171

152. Long K, Su C, Hu C, *et al*. Stretchable, conductive Hydrogel-Based triboelectric nanogenerator integrated with deep learning algorithm for character recognition. *Chem Eng J*. 2024;499:155919.

doi: 10.1016/j.cej.2024.155919

153. Rudin C. Stop explaining black box machine learning models for high stakes decisions and use interpretable models instead. *Nat Mach Intell*. 2019;1(5):206-215.

doi: 10.1038/s42256-019-0048-x

154. Butler KT, Davies DW, Cartwright H, Isayev O, Walsh A. Machine learning for molecular and materials science. *Nature*. 2018;559(7715):547-555.

doi: 10.1038/s41586-018-0337-2

155. Karniadakis GE, Kevrekidis IG, Lu L, Perdikaris P, Wang S, Yang L. Physics-informed machine learning. *Nat Rev Phys*. 2021;3(6):422-440.

doi: 10.1038/s42254-021-00314-5

156. Mahmoudabadbozchelou M, Karniadakis GE, Jamali S. nn-PINNs: Non-Newtonian physics-informed neural networks for complex fluid modeling. *Soft Matter*. 2022;18(1):172-185.

doi: 10.1039/d1sm01298c

157. Chen H, Yang M, Smetana B, Novák V, Matějka V, Compton RG. Discovering Electrochemistry with an Electrochemistry-Informed Neural Network (ECINN). *Angew Chem Int Ed*. 2024;63(13):e202315937.

doi: 10.1002/anie.202315937

158. Tao F, Sui F, Liu A, *et al*. Digital twin-driven product design framework. *Int J Prod Res*. 2019;57(12):3935-3953.

doi: 10.1080/00207543.2018.1443229

159. Tao F, Zhang H, Liu A, Nee AYC. Digital Twin in Industry: State-of-the-Art. *IEEE Trans Ind Inf*. 2019;15(4):2405-2415.

doi: 10.1109/TII.2018.2873186

160. Jamshididana S, Bischoff A, Olarra A, Holmgren B, Roach DJ. Real-time digital twin of vat-based 3D printing using in-situ ultrasonic monitoring. *Virtual Phys Prototyping*. 2025;20(1):e2592734.

doi: 10.1080/17452759.2025.2592734

161. Ng WL, Goh GL, Goh GD, Ten JSJ, Yeong WY. Progress and opportunities for machine learning in materials and processes of additive manufacturing. *Adv Mater*. 2024;36(34):2310006.

doi: 10.1002/adma.202310006

162. Topart J, Tortajada H, Fiolet T, Lombardi R, Panier S. Enabling AI-Controlled additive manufacturing with real-time multiphysics digital twins. *Virtual Phys Prototyping*. 2026;21(1):e2610146.

doi: 10.1080/17452759.2025.2610146

163. Hossain MB, Posada-Quintero HF, Chon KH. A Deep Convolutional Autoencoder for Automatic Motion Artifact Removal in Electrodermal Activity Signals: A Preliminary Study. In: Proceedings of the 2022 44th Annual International Conference of the IEEE Engineering in Medicine & Biology Society (EMBC). July 11-15, 2022; Glasgow, United Kingdom. IEEE; 2022:325-328.

doi: 10.1109/embc48229.2022.9871635

164. Wang C, Guo Y, Han G, Zhou Y, Nyein HYY. Calibration-free and ready-to-use wearable electroanalytical reporting system (r-WEAR) for long-term remote monitoring of electrolytes markers. *Biosens Bioelectron*. 2025;267:116769.

doi: 10.1016/j.bios.2024.116769

165. Armbrust M, Fox A, Griffith R, *et al*. A view of cloud computing. *Commun ACM*. 2010;53(4):50–58.

doi: 10.1145/1721654.1721672

166. Hamid SHA, Hock GC. Rapid prototyping of microstrip patch antenna design: A review and bibliometric analysis for future research directions. *Mater Sci Addit Manuf*. 2025;4(4):025260052.

doi: 10.36922/msam025260052

167. Bariya M, Nyein HYY, Javey A. Wearable sweat sensors. *Nat Electron*. 2018;1(3):160-171.

doi: 10.1038/s41928-018-0043-y

168. Li S, Feng S, Kuan A, Lu Y. Toward a Standard Data Architecture for Additive Manufacturing. *JOM*. 2024;76(4):1905-1912.

doi: 10.1007/s11837-023-06367-4

169. Tang Y, Rahmani Dehaghani M, Wang GG. Review of transfer learning in modeling additive manufacturing processes. *Addit Manuf*. 2023;61:103357.

doi: 10.1016/j.addma.2022.103357

170. Zhao S, Liu S, Jiang Y, *et al*. Industrial Foundation Models (IFMs) for intelligent manufacturing: A systematic review. *J Manuf Syst*. 2025;82:420-448.

doi: 10.1016/j.jmsy.2025.06.011

171. Hu X. Foundation models for physiological data, how to develop them, and what to expect of them. *Physiol Meas*. 2024;45(2):020301.

doi: 10.1088/1361-6579/ad252f